Elsevier Editorial System(tm) for International Journal of Medical Microbiology
Manuscript Draft

Manuscript Number: IJMM-D-13-00280R1

Title: Modelling antibiotic and cytotoxic Isoquinoline effects in Staphylococcus aureus, Staphylococcus epidermidis and mammalian cells

Article Type: Research Paper

Keywords: metabolism; infection; extreme pathway analysis; gene expression; voronoi tessalation; principal component analysis; metabolites

Corresponding Author: Prof. Thomas Dandekar,

Corresponding Author's Institution: University of Wuerzburg, biocenter

First Author: Alexander Cecil , Dr.

Order of Authors: Alexander Cecil , Dr.; Knut Ohlsen, PD Dr.; Thomas Menzel, Dr.; Patrice Francois, Dr.; jacques schrenzel, Dr.; Adrien Fischer, Dr.; Kirsten Dörries; Martina Selle; Michael Lalk, Prof. Dr.; Julia Hantzschmann; Marcus Dittrich , MD PhD; Chunguang Liang , Dr.; Joerg Bernhardt, Dr.; Tobias A Oelschlaeger, Dr.; Gerhard Bringmann, Prof. Dr.; heike Bruhn, Dr.; Matthias Unger , Dr.; Alicia Ponte Sucre , Dr.; Leane Lehmann, Prof.; Thomas Dandekar

Abstract: Isoquinolines (IQs) are natural substances with an antibiotic potential we want to optimize. Specifically, IQ-238 is a synthetic analog of the novel-type N,C-coupled naphthylisoquinoline (NIQ) alkaloid ancisheynine. We developed and tested other IQs such as IQ-143. By utilizing genome-wide gene expression data, metabolic network modelling and voronoi tessalation based data analysis - as well as cytotoxicity measurements, chemical properties calculations and principal component analysis of the NIQs - we show that IQ-238 has strong antibiotic potential for staphylococci and low cytotoxicity against murine or human cells. Compared to IQ-143, systemic effects are less. Most enzyme activity changes due to IQ-238 are located in the carbohydrate metabolism. Validation includes metabolite measurements on biological replicates. IQ-238 delineates key properties and a chemical space for a good therapeutic window. The combination of analysis methods allows suggestions for further lead development and yields an in-depth look at Staphylococcal adaptation and network changes after antibiosis. Results are compared to eukaryotic host cells.

Julius-Maximilians-
UNIVERSITÄT
WÜRZBURG

BIOZENTRUM
UNIVERSITÄT
WÜRZBURG

Dept Bioinformatics,Biocenter, D-97074 Würzburg; Germany

Prof. Dr. Thomas Dandekar

Telefon +49-(0)931 888 4551
Telefax +49-(0)931 888 4552
dandekar@biozentrum.uni-wuerzburg.de
www.bioinfo.biozentrum.uni-wuerzburg.de

To
Prof. Dr. Jörg Hacker
- Editor in Chief -

International Journal of Medical Microbiology
German National Academy of Sciences,
Emil-Abderhalden-Str. 37,
D-06108 Halle
.

Würzburg, 16.10.2014

Ms. Ref. No.: IJMM-D-13-00280

Modelling antibiotic and cytotoxic isoquinoline effects in Staphylococcus aureus, Staphylococcus epidermidis and mammalian cells

Dear Prof. Hacker,

We herewith submit now our revision of the above manuscript. We thank the reviewers for their thoughtful comments which helped to improve the manuscript and submit a point-by-point change list to detail how each of them was incorporated. As you see from the author list and the results in the revision, we included new data covering key points raised by the reviewers.

We hope that the changes will proof satisfactory and look forward to your comments on the revised manuscript.

Sincerely yours
Thomas Dandekar

Reviewer #1 summarizes the results presented and comments: The manuscript provides novel information on the mechanism of action of IQ-238, a compound with antibiotic properties against Staphylococcus. However, the model-based methods used for the study of the effects of the compounds should be empirically validated. In a previous manuscript, the authors validated some of the IQ-143 metabolic induced changes (Cecil et. al., Genome Biol, 2011) by measuring some of the bacterial metabolites after the addition of IQ-143 and confirming for some of the predictions made by the model that they were correct. In this study the effects observed by administration of IQ-238 are different, moreover some of the methodology to reach their conclusions (voronoi tessalation) was not used before. For these reasons the authors should empirically validate some of the model-based conclusions obtained. For example, the authors describe that the voronoi tessalation showed additional changes on the riboflavin metabolism, which they could validate by measuring some of the metabolites that one would expect to be affected by the riboflavin metabolism.
--A: We included now repetition experiments (Figure S2 and S3) and measured specific metabolites directly including nucleotides, carbohydrates and amino acids (Table 6). These support the data including the effects predicted from the modeling. The up- and down regulations of further pathways is explained now including the example given (more active GTP and ribulose-5-phosphate results in a more active riboflavin metabolism, as only the ATP dependent reaction from FMN to FAD shows reduced activity as confirmed by the validation metabolite measurements)

Regarding to this point, the authors describe in the first paragraph of the discussion that "we tested the independence of the data sets carefully and used them also to cross validate the modeled pathway fluxes, e.g. whether the network predictions from gene expression data were fitting measured nucleotide concentrations". Although specified in the discussion, these validations were not shown in this manuscript.
--A: Also this important validation step is now explained in more detail (pp. 14,15) and includes now the new measured metabolite data (Table 6), too.

The authors conclude that IQ-238 has less systemic effects than IQ-143, since IQ-238 only affects to carbohydrate metabolism. However, Voronoi treemaps (Fig. 6) show that IQ-238 have a systemic effect although opposite in most cases to that observed for IQ-143. IQ-238 increased (brown colors) the activity of several pathways, including pathways related to pathogenesis. The discrepancies between the results obtained by both methods should be explained and the increase observed in several pathways by IQ-238 should be validated. For example, prophage functions seem to be upregulated after IQ-238 and this could be easily studied.
--A: These observations do not differ, we only summarized the pathway changes first only focusing on the main pathways affected, carbohydrate metabolism, while the Voronoi treemaps, as the reviewer observed himself, are much more sensitive to detect further changes. However, we completely agree, the reader should be alerted to this and get this properly explained including the conclusions on more systemic effects and how this compares to IQ-143. The manuscript was extended in this respect.

The authors describe IQ-238 to be clearly advantageous over IQ-143 since it only alters the carbohydrate metabolism. Although speculative, one negative effect that could have the narrower effect of IQ-238 is that the bacteria could adapt faster to the presence of IQ-238 and resistance to this compound could emerge more rapidly. Since the authors are comparing both molecules and claim that IQ-238 seems to be a better candidate for their antibiotic properties, it will be good to know to what extend resistant bacteria emerge in the presence of each of these molecules.
--A: Good point, we added more information on resistance development according to our observations as requested. In particular, we report now the results for growth comparing different antibiotic concentrations and resistance development.

The authors used PCA to cluster different IQs by their chemical properties. Then authors describe in the text that IQ-238 point out an island in the plane between the two principal axes where a number of promising lead molecules may be situated. Could the authors identify in the PCA figure which one is the space where good candidate should be found?
--A: Right, this improves the quality of the figure and was added as requested. It is the plane around IQ-238 and IQ-143 which are now similarly colored for easy identification.

Also, could the authors indicate which are the molecules that reside within this space and therefore could be good candidates because of their chemical properties? For example the authors indicate that IQs 370, 281, 251, 324, 283 are viable bioactive candidates with therapeutic windows. These molecules are in different sites within the PCA. Which of these molecules should be considerate as better candidates taking into account the PCA results? Should any of these molecules be studied also in detail as the authors suggested for IQ-238?
--A: The respective position of the IQs becomes now better visible and indicates a clear plane in the PCA where to expect promising substances of the type of IQ-238 and IQ-143. We discuss also behavior of other IQs.

Minor points:

Material and methods, calculation of chemical and biological properties section: antibiotic action is supposed to be described in Table 4?
--A: In the Table we describe Enzyme activities after administration of IQ-238 in *S. aureus* USA300, this is now also corrected and explained in M&M.

Figure 2 could be moved to supplementary.
--A: With the revisions, in particular the new metabolite measurements, the graphical overview on the modelled and measured metabolites turned out to be useful and was kept including revisions of the figure to indicate where validation measurements were done (* in the figure).

When generating the Voronoi trees, why the authors focus on all available genes for IQ-143 and only in main categories of the TIGR database for IQ-238? If authors want to compare both molecules, shouldn't they apply the same methodology for both?
--A: Yes, the reviewer is right, we should have here the same level of resolution for such comparisons and we updated the comparisons accordingly showing only comparable Voronoi trees. You can now compare the gene expression data Voronoi trees and on the same level of detail both for IQ-143 as well as IQ-238. The exact tessalations differ as different changes result from the two IQs.

The font size of some of the text included in the voronoi trees is very small and difficult to read. It will help to have a color legend within the voronoi tree figure to follow better the changes (increase/decrease) in functions described in voronoi trees.
--A: We tried to improve text and font in the voronoi tree figure. Furthermore, we added a color legend as a small bar at the bottom of each voronoi tree.

Table 2. What is the IC50 of 293T cells for IQ-143?
--A: We add now the missing data to the table and made a note for the benefit of the reader.

In the discussion: "We collected all resulting network effects on different enzymes comparing Staphylococcus aureus, S. epidermidis and human and murine cells". Authors should delete human and murine cells in this sentence since they did not analyze the effect of the compound in different enzymes from human and murine cells.
--A: We clarified this statement, the referee is right regarding experimental data apart from

toxicity tests carried out in human and murine cells, but we actually modeled the resulting network effects also for human and murine cells.

In the discussion: it probably will be good to change "man" for human
--A: done as requested.

When the authors reconstruct the metabolic networks and do PCRs to detect additional enzymes for *S. epidermidis* (Fig.S1), have the authors sequenced the PCR products to corroborate the presence of those particular enzymes?
--A: We have only checked if the PCR products had the expected size and, of course, that the primer sequences did prime and produced the predicted bands. However, this is now also clarified in the text of the supplementary file.

In supplementary materials index, "enzmyes" should be enzymes.
--A: done as requested.

Why in Fig. 7 compound IQ-143 is purple and IQ-238 is orange if both of them have activity against bacteria?
--A: We changed the color of the compound IQ-143 to orange in accordance with the findings we previously published.

In the methods section Functional clusters by Voronoi tree analysis: (Figures 7 to 9) should be replaced by Figures 4 to 6.
--A: done as requested.

Besides, when authors describe in the methods: "Expression ratios (log ratios of IQ-143 treated IQ-143 S. epidermidis vs. control and log ratios of IQ-238 treated S. aureus) were mapped as colors". Does this mean that voronoi tree maps were performed for IQ-143 effects on *S. epidermidis* and for IQ-238 for S. aureus? If this is true, why did not the authors compare the effect of both molecules on the same Staphylococcus species?
--A: We show now always the same resolution for the Voronoi tree maps in the paper and together with the supplementary material one can easily compare IQ-143 and IQ-238 effects according to the Voronoi tree maps both for *S.aureus* and *S.epidermidis*. A color code is given by a bar at the bottom. Furthermore, Gene expression analysis in the presence of inhibitory and subinhibitory concentrations of IQ-143 were performed previously with S. epidermidis due to the access to DNA-microarrays of this species. Here, we investigated the impact of IQ-238 on gene expression of *S. aureus* as the more relevant pathogenic species. Given a similar activity of IQ-238 against both species the mode of action of this compound is probably the same in both species (all currently used anti-staphylococcal antibiotics have the same mechanism of action in both species).

Material and methods section "calculation of chemical and biological properties": there is no Figure 10 and Figure 11. Please correct.
--A: done as requested, refers to Figure 7 and 8 in fact.

Could Figure 3 legend be improved by containing the word "on" or "of" between modeling and S. aureus?
--A: done as requested.

Staphylococcus is a non-spore forming bacteria, however one of the pathways that is increased after IQ-238 is sporulation and germination (brown colors in Fig. 6). Is this due to an error when defining the functions or actually Staphylococcus has some functions involved in sporulation and germination?
--A: The coloring was done according to TIGR classification and not according to *S.aureus*

functional categories. *S.aureus* has protein homologues of these classes but is not doing active sporulation or germination.

Results section: PCA: Evaluation of IQ-properties: (Figure 1) does not seem to fit well with the text.
--A: Right - deleted as requested

The first paragraph of the discussion: "This work demonstrates how network modelling can help to supplement missing information and how metabolic modelling allows predictions on the enzyme activities of the complete network with implications for the action of the modelled compound". The authors already demonstrated this in their previous paper (Cecil, et al. Genome Biol, 2011) so the information of this paragraph should refer to their previous paper.
--A: Yes, we quite agree, we added this citation as requested and put it also in context (further citation).

Reviewer #2 commented that the search for new antibiotics is an urgent challenge and considered our manuscript an interesting study that deserves attention but needs follow up experiments.

Major concerns/questions:
- what about the primary target of IQs? In my opinion the conclusions of the paper are not convincing!
--A: We agree that the primary mode of action of the IQs is not finally determined. However, we think the results of the study show how gene expression data combined with metabolic modelling, as well as with the inclusion of metabolomics data are powerful tools to get an overview on possible mechanisms of action which have to be confirmed further in follow-up studies. Therefore, we included now metabolite changes to get more information to primary targets of IQs. This important information is now added to the manuscript. Furthermore, we tried to phrase our conclusions more carefully and discuss the predicted primary targets in a critical way according to all our experimental results.

- to understand the mode of action data on basic physiology have to be presented such as a detailed growth kinetics after the application of the substances (0 to 60 min), the composition of the growth medium (particularly glucose concentration etc. - did I miss the information?). This kind of physiological data is the fundament for all conclusions.
--A: A very well taken suggestion, we added now this information in much more detail in the materials and methods section such as more detail on media composition and included information on the growth kinetics, glucose concentration and glucose consumption in figure S2 and figure S3.

- in case there is a rapid stop of growth a strong down regulation of genes whose products are crucial for growth (e.g. ribosomal proteins etc.) is expected. Please, comment.
--A: As shown in Figure S2, IQ-238 acts bacteriostatic resulting in a delayed reduction of growth. There is no rapid stopping of growth. Moreover, a strong down-regulation of ribosomal proteins is not supported by gene expression data.

- -to the down regulation of the expression of glycolytic genes: it is surprising that genes that are located in one operon do not show similar results (e.g. eno operon encoding gapA etc.). Is there any influence on the uptake of glucose?

--A: Another good comment, we now include information on glucose uptake as well as on how operons behave such as the eno operon encoding gapA and whether enzymes from the same operon can also behave differently in their changes. Also, the glucose uptake by PTS permease 1 and 2 is calculated to be reduced in *S. epidermidis* by 45%. In *S. aureus* the uptake by PTS permase 1 doubles, whereas the uptake by PTS permase 2 is reduced by 35%.

- see Discussion: "As shown, the glycolysis is particularly affected. The gene expression for the fructose-bisphosphatase, 6-phosphofructokinase, aldolase and GapDH are downregulated." This is very surprising: first - the first enzyme is NOT a glycolytic enzyme (gluconeogenesis - the opposite!). Second - I doubt that glycolytic enzymes and gluconeogenetic enzymes are regulated in the same way!
--A: We went over this important point again, in particular the accurate enzyme reactions modelled and pathway reactions and discuss now also the point made, whether there is general dysregulation after GBAP238 and find, perhaps more coherently, only the glycolysis is in particular down regulated while few other enzymes are also affected.

- It would be interesting to validate the data on enzyme activities by direct enzyme activity measurements (for dehydrogenases this is quite simple).
--A: We validated many of the data now by direct metabolite measurements, the detailed data are given in supplementary material and key observations are given in the results and discussed, the author-list has been extended accordingly.

- What is "general stress response"? Probably not the SigB-dependent reaction of S. aureus!
--A: We apologize for the phrasing, there is no general stress response, we give now a clear list on the selected few stress response genes affected.

Modelling antibiotic and cytotoxic Isoquinoline effects in *Staphylococcus aureus, Staphylococcus epidermidis* and mammalian cells

Alexander Cecil[1,#], Knut Ohlsen[2,#], Thomas Menzel[2], Patrice François[3], Jacques Schrenzel[3], Adrien Fischer[3], Kirsten Dörries[4], Martina Selle[2], Michael Lalk[4], Julia Hantzschmann[2], Marcus Dittrich[1], Chunguang Liang[1], Jörg Bernhardt[5], Tobias A. Ölschläger[2], Gerhard Bringmann[6], Heike Bruhn[2], Matthias Unger[7], Alicia Ponte-Sucre[8], Leane Lehmann[7], and Thomas Dandekar[1,9,*]

1. Department of Bioinformatics, Biocenter, University of Würzburg, Am Hubland, 97074 Würzburg, Germany.
2. University of Würzburg, Institute for Molecular-Infection Biology, 97070 Würzburg, Germany.
3. Genomic Research Laboratory, Service of Infectious Diseases, University of Geneva Hospitals, Rue Gabrielle-Perret-Gentil 4, CH-1211 Geneva 14, Switzerland, Geneva.
4. Institute of Biochemistry, Ernst-Moritz-Arndt-University Greifswald, Felix-Hausdorff-Straße 4, D-17487 Greifswald, Germany.
5. Institute for Microbiology, Ernst-Moritz-Arndt-University Greifswald, Friedrich-Ludwig-Jahn Strasse 15, D-17487 Greifswald, Germany.
6. University of Würzburg, Institute for Organic Chemistry, Am Hubland, 97074 Würzburg, Germany.
7. University of Würzburg, Institute for Pharmacy and Food Chemistry, Am Hubland, 97074 Würzburg, Germany.
8. Laboratory of Molecular Physiology, Universidad Central de Venezuela, Caracas, Venezuela
9. EMBL Heidelberg, BioComputing Unit, Meyerhofstraße 1, 69117 Heidelberg, Germany.

[#] These authors contributed equally to this work.

* Corresponding author. Department of Bioinformatics, Theodor-Boveri-Institute of Life Sciences, University of Würzburg, Am Hubland, 97074 Würzburg, Germany.

Tel.: +49 931 3184551; Fax: +49 931 3184552;

Email: dandekar@biozentrum.uni-wuerzburg.de

Supplementary information is available at

http://bioapps.biozentrum.uni-wuerzburg.de

Abstract

Isoquinolines (IQs) are natural substances with an antibiotic potential we aim to optimize. Specifically, IQ-238 is a synthetic analog of the novel-type N,C-coupled naphthylisoquinoline (NIQ) alkaloid ancisheynine. Recently, we developed and tested other IQs such as IQ-143. By utilizing genome-wide gene expression data, metabolic network modelling and voronoi tessalation based data analysis – as well as cytotoxicity measurements, chemical properties calculations and principal component analysis of the NIQs – we show that IQ-238 has strong antibiotic potential for staphylococci and low cytotoxicity against murine or human cells. Compared to IQ-143, systemic effects are less pronounced. Most enzyme activity changes due to IQ-238 are located in the carbohydrate metabolism. Validation includes metabolite measurements on biological replicates. IQ-238 delineates key properties and a chemical space for a good therapeutic window. The combination of analysis methods allows suggestions for further lead development and yields an in-depth look at staphylococcal adaptation and network changes after antibiosis. Results are compared to eukaryotic host cells.

Keywords: metabolism; infection; extreme pathway analysis; gene expression; voronoi tessalation; principal component analysis; metabolites;

Introduction

Lead candidates for novel antimicrobial compounds have been found within a new subclass of bioactive natural products, the N,C-coupled naphthylisoquinoline (NIQ) alkaloids (Yang et al., 2003; Bringmann et al., 2006), which were first isolated from tropical lianas (Bringmann et al., 2006) belonging to the Ancistrocladaceae plant family. Representatives of these alkaloids such as ancistrocladinium A and B (Bringmann et al., 2010) exhibit excellent anti-infective activities against infections with *Leishmania major* but have low side-effects. They thus serve as promising lead structures (Bringmann et al., 2010) for the treatment of severe infectious diseases.

IQ-238 is a dimeric N,C-coupled naphthylisoquinoline. It has minor structural differences, consisting of an amide group located at the carbon 4' in comparison to IQ-143 (Figure 1). It has been identified by structure-activity relationship (SAR) studies (Ponte-Sucre et al., 2009) in a screening program for compounds with anti-staphylococcal activity (Bringmann et al., 2007). This class of compounds, comprised of complex natural products and newly developed synthetic analogues thereof (Ponte-Sucre et al., 2007; Ponte-Sucre et al., 2010), provides a rich repertoire of representatives with a large potential against a number of infectious disease pathogens, but some of them bear the risk of toxic effects to humans (Cecil et al., 2011).

Antibiotic treatment in infectious diseases has become increasingly challenging as pathogenic bacteria have acquired a broad spectrum of resistance mechanisms. In particular, the emergence and spread of multi-resistant staphylococci progressed to a global health threat (Grudmann et al., 2010). They are not only resistant to almost all treatments, they also adapt very well to different conditions in the host, e.g. by persistence (Wright el al, 2010; Cheng et al., 2009; Mattner et al., 2010). In the face of increasing resistances against antibiotics an intensive search of new antibacterial lead compounds addressing new targets is urgently

demanded.

In our study we start from an isochinoline, the antibacterial compound IQ-238 which exerts antibacterial activity against a broad range of Gram-positive pathogens including staphylococci and streptococci. Gene expression analysis, metabolic modelling and cytotoxicity assays are combined to show its promising properties as an antibiotic lead against *Staphylococcus aureus* and *Staphylococcus epidermidis.* Metabolic modelling allowed considering all flux and metabolic changes of the central metabolism, including enzymes where gene expression did not change significantly. Combined data indicate that IQ-238 is a promising lead as it interferes in both staphylococcal species with central carbohydrate metabolism as well as the citric acid cycle (TCA cycle), electron transport, and amino acid biosynthesis but has low toxicity in human or murine cells.

For improved evaluation of lead structures, further analysis methods include Voronoi tessalations. These regard TIGRFam gene functional classification and hierarchy of affected gene expression changes to reveal subtle network changes from gene expression data. This method showed additional restrained changes in the staphylococcal riboflavin metabolism for the previously investigated lead compound IQ-143. Also in this analysis method IQ-238 compares well to IQ-143 regarding therapeutic window with its spectrum of changes mainly located in the carbohydrate metabolism of staphylococci. This is confirmed on biological replicates by direct metabolite measurements.

Comparing all results, a more general perspective on NIQ compounds is achieved by a principle component analysis (PCA) of the physicochemical properties. This allows an assessment of the antibiotic potential as well as toxic risk for different NIQs already tested and thus yields recommendations for further lead improvement.

Materials and Methods

Isolation of RNA:

For the isolation of total RNA for microarray experiments, *S. aureus* strain HG001 was grown to mid-log phase at an optical density at 600 nm of 0.6 to 0.8. In case of addition of IQ-238, 10 x MIC were supplemented. After incubation for another hour, 7 ml of bacterial culture were mixed with 7 ml of RNAprotect™ Bacteria Reagent (Qiagen, Hilden, Germany) and immediately incubated on ice. After centrifugation for 10 min at 6.000 x g and 4°C, the supernatant was discarded and the pellet resuspended in 1 ml RLT-buffer (Qiagen) supplemented with 1 % (vol/vol) β-mercaptoethanol. Cells were disrupted in Lysing Matrix E (MP Biomedicals) using a FastPrep®-24 (MP Biomedicals, Solon, OH, USA), followed by cooling on ice for 2 min. After brief centrifugation, the supernatant was purified using RNeasy®Mini Kit (Qiagen). To obtain pure RNA, the eluate was treated with DNase (Roche, Grenzach-Wyhlen, Germany) for 1 h at 37°C and again purified with RNeasy®Mini Kit. For RNA-precipitation, 1/10 of sample volume of aqueous sodium acetate solution (3 M, pH 4.8) and 2.5 volumes of cold 100 % ethanol were added and samples incubated for 2 h at -80°C. After centrifugation (15 min, 11.000 x g, 4°C) the supernatant was carefully discarded, the pellet washed with 70 % cold ethanol and dried at room temperature.

Microarray design:

The microarray was manufactured by in situ synthesis of 10,807 oligonucleotide 60-mer probes (Agilent, Palo Alto, CA, USA), selected as previously described (Charbonnier et al., 2005). It covers > 98 % of all ORFs annotated in strains N315 and Mu50 (Kuroda et al., 2001), MW2 (Baba et al., 2002) and COL (Gill et al., 2005), NCTC8325, USA300 (Diep et al., 2006), MRSA252 and MSSA476 (Holden et al., 2004) including their respective plasmids.

Expression microarrays:

For labelled nucleic acids preparation, *S. aureus* strains were grown and total RNA was extracted as described above. After additional DNase treatment, the absence of remaining DNA traces was evaluated by quantitative PCR (SDS 7700; Applied Biosystems, Framingham, MA) with assays specific for 16S rRNA (Renzoni et al., 2006; Scherl et al., 2006). Batches of 5 µg total *S. aureus* HG001 RNA were labeled by Cy-3dCTP (without IQ-238) or with Cy-5 dCTP (with IQ-238) using the SuperScript II (Invitrogen, Basel, Switzerland) following manufacturer's instructions. Labeled products were then purified on QiaQuick columns (Qiagen). Labeled cDNA mixture was diluted in 50 µl Agilent hybridization buffer, and hybridized at a temperature of 60°C for 17 hours. Slides were washed with Agilent proprietary buffers, dried under nitrogen flow, and scanned using 100 % photo multiplier tube power for both wavelengths.

Microarray analysis:

Fluorescence intensities were extracted using Feature extraction software (Agilent, version 8). Local background-subtracted signals were corrected for unequal dye incorporation or unequal load of the labeled product. The algorithm consisted of a rank consistency filter and a curve fit using the default LOWESS (locally weighted linear regression) method. Data from two independent biological experiments were expressed as Log10 ratios and analyzed using GeneSpring 8.0 (Silicon Genetics, Redwood City, CA, USA). The statistical significance of differentially expressed genes was identified by variance analysis (ANOVA) (Churchhill, 2006), performed using GeneSpring, including the Benjamini and Hochberg false discovery rate correction of 5% (P value cutoff, 0.05) and an arbitrary cutoff of 1.5fold for expression ratios. The complete microarray dataset has been posted on the Gene Expression Omnibus database http://www.ncbi.nlm.nih.gov/geo/, accession number GPL11137 for the platform design and GSE33832 for the original dataset.

Reconstruction of metabolic networks:

To model involved metabolic pathways we used the database KEGG (Kanehisa et al., 2008). Additional genome annotation of missing enzyme

activities for the central pathways applied iterative sequence and domain analysis methods (Gaudermann et al., 2006). Subsequent experimental verification by PCR complemented this (see supplementary Figure 1 and supplementary Tables S2, S3). We tested whether the PCR products had the expected size and, that the primer sequences did prime and produced the predicted bands. The model of the central metabolism included - besides lipid and amino acids – the central carbohydrate metabolism as well as nucleotide and salvage pathways.

Metabolic flux modelling:

Extreme pathways possible in the annotated enzyme network were calculated first (Schuster et al., 2000). To identify actual flux strengths we applied YANAsquare and a custom written program in R (Gentlemen and Ihaka 1996). We modelled flux strengths the metabolic webs of *S. aureus* USA300 and *S. epidermidis* RP62A to gene expression data obtained for the purpose (supplementary Table S1). A least square fit used first YANAsquare and next the improved R routine to calculate optimal pathway fluxes that best matched the constraints for key enzyme activities as estimated according to significant elevated or lowered enzyme expression in the above data sets (Table 1, Supplementary Table S1).

Detailed input files for the pathway models are listed in additional file 1: *S. aureus* USA300 (supplementary Table S4), *S. epidermidis* RP62A (supplementary Table S5). The calculated activities of the different extreme pathway modes (EMs) for one or two different concentrations of IQ-238 for the respective organisms: *S. aureus* (supplementary Tables S6), *S. epidermidis* (supplementary Tables S7).

IC50 determination for host cells:

J774.1 macrophages (a murine cell line) were cultured in complete medium (RPMI with $NaHCO_3$, 10% FCS, 2 mM glutamine, 10 mM Hepes pH 7.2, 100 U/ml penicillin, 50 µg/ml gentamicin, 50 µM 2-mercaptoethanol) without phenol red in the absence or presence of increasing concentrations of the compound at a cell density of 1×10^5

cells/ml (200 µl) for 24 h at 37 °C, 5% CO_2 and 95% humidity. Following the addition of 20 µl of Alamar Blue, the plates were incubated and the ODs measured at 24 h, 48 h, and 72 h. The standard Alamar blue assay as previously described was followed (Pimentel-Elardo et al., 2010).

Human Kidney epithelial 293T cells (2 × 104 cells/ml; human embryonal kidney cells HEK 293 transformed additionally with SV40 large T-antigen) were tested in the same manner as the macrophages except that complete DMEM medium was used: 4.5 g/l solution of DMEM high D-glucose solution with sodium pyruvate but without L-glutamine, FBS superior at final concentration of 20%, 200 mM L-glutamine 100x.

Functional clusters by Voronoi tree analysis:

For global gene expression analysis we used Voronoi Treemaps as described previously by Bernhardt et al. (2009) and Otto et al. (2010).

This type of visualization can display hierarchically structured data such as functional categories of *Staphylococcus* strains according to TIGRFams categorization in a space filling manner (Figures 4 to 6). The different treemap clusters correspond to the main category and sub category level of TIGRFams. To make an interstrain comparison of *S.aureus* and *S.epidermidis* possible we constructed an all S. *aureus* and *S. epidermidis* strains containing treemap with the TIGR main category level at first, the TIGR sub category level at second, their operon structure (Price et al., 2005; Price et al., 2005) predictions at third and the corresponding TIGR locus tag IDs at fourth level.

If available, locus tag IDs were replaced by traditional gene names from microbes online or from orthologue clusters gene names given in MBGD Microbial Genome Database (Uchiyama, 2003; Uchiyama, 2007; Uchiyama et al., 2010). Expression ratios (log ratios of IQ-143 treated *S. epidermidis* vs. control and log ratios of IQ-238 treated *S. epidermidis*) were mapped as colors (orange for upregulation, grey for unchanged

expression and blue for down regulation) onto gene tiles. Homogeneously up- or down regulated gene clusters illustrate the involved cellular functions during IQ-treatment.

Calculation of chemical and biological properties:

The chemical properties of the naphtyhlisoquinolines (Table 5) were calculated by applying ChemAxon's “MarvinSketch” (Marvin Version 5.5.1.0, ChemAxon, Záhony u. 7, Building HX, 1031 Budapest, Hungary. [http://www.chemaxon.com]) according to their respective chemical structure files. Properties considered included the polar surface area; the molecular weight; the octanol-water coefficient (logP- defining the uptake ratio of the compound into the organisms or cell types) as well as H-bond donors and acceptors. To fulfill Lipinski´s rule of 5, the following criteria must be met: not more than 5 H-bond donors, not more than 10 H-bond acceptor, a molecular weight not larger than 500 Dalton, and logP not greater than 5. From this data (Table 5), compounds were separated by analysis of maximum variance according to the first two components (Figure 7). In Figure 8 the toxicity according to IC_{50}- values against J774.1 macrophages is considered and separation according to PCA calculated. Perl scripts calculated the PCA (correlation to H-donors, Polar surface, H-acceptors, logP, rings, molecular weight and atoms). These were derived from the vegan package (Oksanen et al., 2010) and adapted to our needs.

Metabolite Measurements:

To validate the *in silico* predictions we measured intracellular and extracellular metabolites. To this end we created four biological replicates: *S. aureus* HG001 was grown in B-medium and exposed to IQ-238 (10xMIC) at an OD600 nm of 0.7. Metabolome samples were taken directly after 60 min and 120 min after treatment (Supplementary Figure S2). All metabolite data (extracellular and intracellular) were acquired from the respective strain as described earlier (Dörries et al., 2014). Briefly, for the analysis of extracellular metabolites (glucose, trehalose), culture supernatant was sterile filtered and analyzed by using ^{1}H-NMR spectroscopy as described by Dörries et al., 2013 (Supplementary Figure S3). Intracellular metabolites were analyzed by using GC-MS and HPLC-MS techniques. For it, 15 OD units of the

bacterial culture were sampled using the fast vacuum dependent filtration as described elsewhere (Dörries et al., 2014). Sample preparation and the subsequent analysis of intracellular metabolites was done as previously described (Dörries et al., 2014). In doing so, metabolite identification and integration resulted in relative metabolite amounts per 7.5 OD units. Growth phase-related intracellular metabolite changes were excluded by calculating the fold changes (FC) of all relative metabolite amounts at every sampling time point (t_{60} and t_{120}) divided by the corresponding metabolite amount at time point zero for both, untreated and stressed cells. Statistically significant differences in metabolite FC between stressed and untreated cells of 4 biological replicates were calculated using unpaired t-test (Table 6).

Results

IQ-238 driven gene expression changes in Staphylococci:

To get a first picture on the genome-wide effects of IQ-238 on staphylococci DNA-microarray experiments were conducted. *S. aureus* strain HG001 (Herbert et al., 2010) was grown in the presence of 10 x MIC IQ-238 as described in the material and methods section and hybridized to microarrays containing eight complete *S. aureus* genomes. Significant gene expression differences for *S. aureus* after cultivation with inhibitory concentrations of IQ- 238 are shown in Table 1 (and all results in supplementary material Table S1). Genes encoding proteins involved in the central carbohydrate metabolism like the glucose-6P-isomerase, the fumarate hydratase and the L-lactate dehydrogenase are significantly down regulated by the presence of IQ-238 in the growth medium. In addition, efflux transporters like the formate/nitrite-transporter, the choline/betaine/carnitine transporter and the multi-drug transporters are all significantly up-regulated. Only few stress response genes were activated by IQ-238. Specifically, this involved activation of genes encoding for capsular polysaccharide synthesis enzymes (gene names: *capG*, *capH*, *capI*, *capJ*, *capK*, *capL*, *capM*, *capN*, *capO*) as well as the cold shock protein cspB was observed. The fold- changes (WT w IQ-238 vs. WT w/o IQ-238) range from 2.99 to 3.88 for those genes.

Integrated model of IQ-238 effects considering metabolic flux changes:

In order to get a more complete overview from these gene expression data, we built a metabolic model of the involved pathways. For this we started by utilizing available genome sequences (Gill et al., 2005; Diep et al., 2006) and combining those with biochemical data from the Kyoto Encyclopedia of Genes and Genomes (KEGG) database (Kanehisa et al., 2008) as well as further data from a recent own annotation effort (Cecil et al., 2011) to assemble an enzyme network. We then calculated a metabolic flux model, balancing metabolites in the enzyme network, applying YANAsquare (Schwarz et al., 2005; Schwarz et al., 2007) and YANAvergence (Liang et al., 2011).

Our staphylococcal models (Figure 2) include the complete central metabolism: energy and nucleotide metabolism, amino acid metabolism and biosynthesis and degradation of fatty acids. Several transport and protective mechanisms (multi-drug transporter e.g.) were also included.

In previous work (Cecil et al., 2011; Zirkel et al., 2012) we were able to show that fitting gene-expression data directly to many enzymes in a metabolic network model is an accurate way to calculate the overall activities of all enzymes in a given network (calculation error only a few percent). Thus, in a second step, we fitted the network fluxes according to the available gene expression information. By these means, all enzyme activities of the network were calculated – including those without significant changes in their transcript expression level. As a result, the list of changes in enzyme activities and metabolic flux variations becomes more apparent.

Enzymes with a significantly lower activity according to gene expression data and metabolic modelling after administration of the compound include: Phospho-D-glycerate-2,3-phosphomutase (glycolysis), 2-phospho-D-glycerate-hydro-lyase (glycolysis), 6-phosphofructokinase

(glycolysis), phosphoglycerate-kinase (glycolysis), the PEP carboxylase (TCA-cycle) and furthermore the fructose-bisphosphatase (gluconeogenesis, pentose phosphate cycle), which by itself has its flux down-regulated by more than 90%. From these central carbohydrate enzymes the glycolytic enzymes 6-phosphofructokinase, aldolase and glyceraldehyde 3-phosphate dehydrogenase are easily detected by high gene expression changes, the other enzyme changes become apparent by more detailed analysis and metabolic modelling. Enzyme activities from operons such as the gapA operon encoding glyceraldehyde-3-phosphate dehydrogenase A (in contrast to gapA2/ gapB which is gluconeogenic in staphylococci, Fillinger et al., 2000), are in general similar affected, as can also be seen by the Voronoi plots depicting similar categories also with similar colors. There is also an influence on the uptake of glucose by IQ-238: the glucose uptake by PTS permease 1 and 2 is calculated to be reduced in *S. epidermidis* by 45%. In *S. aureus* the uptake by PTS permase 1 doubles, whereas the uptake by PTS permase 2 is reduced by 35%. Further changes revealed by metabolic modelling are indicated by unstippled boxes (Figure 3).

Compared to the previously investigated IQ-143, the modified compound IQ-238 appears clearly advantageous - showing mainly alterations of the carbohydrate metabolism and no strong stress response. This is also seen by the lower cytotoxicity on human or murine cells. Nevertheless, systemic and neurological toxicity has still to be reduced; IQ-238 is only a lead substance and can be refined as outlined below exploiting our combination of modelling methods.

Voronoi treemaps:

IQ-238 changes according to functional clusters in Voronoi treemaps were applied to reveal additional subnetworks affected by IQ-238. Treemaps were coloured considering TIGRFam terms and their hierarchical classification so that clusters of functional related proteins show up if they change together. The mathematical method applied dissects the area of all SA proteins accordingly (“tesselations”) and is called a Voronoi tree graph.

For direct comparison of the IQ effects on gene expression, Voronoi diagrams were generated comparing affected pathways for different concentration dependent effects of IQ-143 on S. epidermidis RP62A (2.0 x MIC as well as 0.25 x MIC) (Figures 4, 5) and IQ- 238 on S. aureus HG001 (10.0 x MIC) (Figure 6). We also calculated and considered Voronoi treemaps as given by flux values for IQ-143 and S. aureus USA300 (supplementary figures S4 and S5) as well as S. epidermidis RP62A for IQ-238 (supplementary figure S6) to make sure that the dominating differences seen are between the IQs. One can confirm that the differences in the Voronoi treemaps between S. epidermidis RP62A and S. aureus HG001 are comparatively small for the same environmental condition. A colour code at the bottom of the treemap indicates up-regulation (orange) or down-regulation (blue). In this way we could focus on the most promising enzyme categories that displayed activity changes in their gene expression. We noted previously direct effects of compound IQ-143 on oxidative phosphorylation (complex 1) and nucleotide metabolism, as well as compensatory effects on complex 3 of the oxidative phosphorylation and energy metabolism in general (Cecil et al., 2011).

Voronoi treemaps give additional insights on network effects as they combine the gene expression values with functional information and hierarchical classification. The lower level terms that belong to a higher level TIGRFam role are together around one common centre of weight using Euclidian metrics. The obtained results are complementary to the above methods; the TIGRFam roles capture pathways and network interactions according to the functional hierarchy of these terms. This classification is sometimes less detailed and in general less specific as the metabolic pathway calculations above but independent from it. The hierarchical clustering of TIGRFam roles and corresponding networks reveals additional subtle network changes. Furthermore, common patterns of network change can be readily recognized by visual inspection of the complex coloured treemaps, a pattern recognition task where humans still excel compared to machine-learning approaches. This technique reveals a number of differences between both IQ compounds (IQ-238, IQ-143) which only become apparent by this analysis method.

The Voronoi diagrams (Figures 4, 5) depict strong down regulation (blue) of citric acid cycle and, to a lesser extent, glycolysis after IQ-143 administration. Both voronoi diagrams thus support previously performed metabolic modelling for this compound. However, the Voronoi diagrams show an up regulation of riboflavin synthesis (brown area in the B-vitamines / cofactor synthesis part in Figure 4 and 5) which was not recognized before by metabolic network modelling. The lower concentration of 0.25 x MIC of IQ-143 showed weaker effects, and the results and changes are again similar to those found for metabolic modelling with 0.16 µM IQ-143 (Cecil et al., 2011).

For IQ-238 Voronoi treemap analysis (Figure 6) reveals strong effects (at concentrations of 10x MIC and higher) on the energy metabolism in *S. aureus*, in particular in the glycolysis and subsequently in the metabolism of NADP/NADPH, the carbohydrate metabolism and the degradation pathways. Here the Voronoi tree maps show also secondary effects besides glycolysis which are not so easy apparent by other modelling techniques. This was subsequently reconfirmed performing a Voronoi treemap analysis on all first level TIGR terms and considering all gene expression values. Further gene categories did not experience prominent gene expression changes (in particular, a general stress response was not observed. Only some stress response genes did change).

Applying all these methods and looking at subtle changes triggered by either compound suggests that IQ-238 is a better lead compound than IQ-143: IQ-238 has strong antibiotic potential for staphylococci and low cytotoxicity against human or murine cells (Table 2). Systemic effects are less pronounced than observed for IQ-143 and there are strong effects on carbohydrate metabolism. Furthermore, there is a good therapeutic window for IQ-238 considering its effects on human cells compared to staphylococci.

Validation by direct metabolite measurements

For a further validation of the predicted (different modelling methods) and observed (gene expression data) changes in enzyme expression and pathway activities, metabolites were directly measured in four biological replicates. The measured metabolites are summarized in Table 6, they cover various metabolites for all the sections of primary metabolism considered in the steps before (Figure 2). Detailed growth kinetics of the experiments are given in Supplementary Figures S2 and the consumption of the carbohydrates trehalose and glucose under the test conditions is shown in Supplementary Figure S3. Addition of 10XMIC of IQ238 reduced the growth of *S. aureus* HG001, however, led not to an immediate stop of cell division. Obviously, ribosomal protein production is not strongly affected. Trehalose (supplementary figure S3-A) composes the main C-source, glucose (supplementary figure S3-B) is already completely consumed before an OD_{600nm} 0.7 is reached (see supplementary figure S2). Taking the different growth rates into account (stress and control over all four different replicates), the uptake of trehalose (supplementary figure S3-C) is the same under stress and control conditions.

The findings are conform and support the conclusions of the *in silico* modelling and gene expression data:

Inhibition of lower glycolysis affects two important metabolic processes: formation of pyruvate and acetyl-CoA as well as the formation of NADH and NADPH by the glyceraldehyde-3-P-dehydrogenase. As shown in Table 6, ATP is depleting over time due to a TCA cycle receiving less acetyl-CoA. A secondary effect can be seen in the accumulation of NADP+.

This leads to a depletion of ATP by affecting the flux through the oxidative phosphorylation (Table 7). Other nucleotides (e.g. GTP and CTP) are accumulating over time as the energy dependent drain reactions for these nucleotides will not perform as efficient as before administration of IQ-238.

The up-regulation of the riboflavin metabolism, as seen in the voronoi tesselations, are supported by the metabolite measurements:

more availabe GTP and ribulose-5-phosphate results in a more active riboflavin metabolism in general, as most reactions are not ATP dependent. Only the ATP dependent reaction from FMN to FAD shows reduced activity, this is confirmed by the measured lower FAD quantities.

PCA: Evaluation of IQ- properties

To obtain more information on how to develop IQs and NIQs further, a more direct comparison of different and already synthesized compounds (such as IQ-143 and IQ-238) regarding their antibiotic effects versus their toxicity was conducted by a principal component analysis (PCA). Chemical properties were calculated according to Lipinski's rule of five (see M&M). Antibiotic properties (also M&M) were evaluated against principal component analysis of chemical properties (Figure 7). The toxicity (M&M) was also compared accordingly to the best separating principal components versus the chemical properties (Figure 8).

IQ-238 has – compared to IQ-143 – a smaller octanol-water-coefficient and a higher polar surface charge, which in turn leads to a more hydrophilic compound. As a result, this compound is more likely not to pass the blood-brain-barrier. Also the transport into cells by diffusion through membranes is less likely to occur. Therefore, neglecting additional complexities such as absorption and partitioning in the body, the PCA analysis suggests again that toxic side effects are likely to be less compared to IQ-143. These improvements of IQ-238 over IQ-143 are also detected against the background of other NIQs tested (Figures 7, 8). For the other compounds we visualize viable bioactive candidates with therapeutic windows (IQs 370, 281, 251, 324, 283), toxic candidates (IQs 353, 335, 336, 304, 265, 314, 278, 277, 276, 274, 279, 285, 275, 361) as well as candidates with good tolerance but no strong antibiotic effect (IQs 268, 310, 299, 309, 300, 334, 324, 339).

Taking all data into account, the chemical properties of IQ-238 point out an island in the plane between the two principal axes where a number of promising lead molecules may be situated. According to this consideration

the phenolic moiety of IQ-238 has to be made more hydrophobic at substituent R1 and we need a donor function – as evidenced for IQ-238 – probably at moiety R2. We stress that this is a speculative suggestion which certainly needs detailed confirmation by further experiments, however this suggestion considers the experimental data collected here and the specific changes of IQ-238 properties compared to IQ-143 and the general properties of NIQs analyzed.

Further improvement of IQ-lead compounds

One such suggestion would be the inclusion of an additional OH group in the molecule, probably in the link that has been included because of the amide will make the compound less prone to go through the blood brain barrier. Modifications to achieve a pro-drug form of IQ-238, e.g. by inclusion of an ester to be cleaved only inside *S.aureus* and transformed there back to a ketone should also be considered. However, the method combination detailed here is applicable to any compound where an improvement regarding its therapeutic window is desirable and gene expression and toxicity data are available.

Discussion

Network modelling shows detailed drug effects

This study, as well as a previous works (Cecil et al., 2011; Zirkel et al., 2012), demonstrates how network modelling can help to supplement missing information and how metabolic modelling allows predictions on the enzyme activities of the complete network with implications for the action of the modelled compound. Gene expression data are complemented by network modelling and counter regulation by higher gene expression can be identified by this methodology. Only a few metabolite measurements are sufficient to validate the predictions regarding involved pathways, e.g. here regarding nucleotides as well as nucleotide containing cofactors. We tested the independence of the data sets carefully and used them also to cross validate the modeled pathway fluxes, e.g. whether the network predictions from gene expression data were fitting measured nucleotide

concentrations (data in results, section validation).
Voronoi tessalations with hierarchical clustering of gene functions revealed further pathway changes not apparent by the other methods, and the same conclusion applies for the exploration of the chemical space available for the optimized lead by PCA.
In general, network modelling allows to consider network effects besides target effects, for instance on glycolysis as well as to identify areas comparatively robust to the antibiotic effects (e.g. TCA cycle).

Metabolic effects of NIQs

Our results suggest that IQ-238 targets the carbohydrate metabolism of *S. epidermidis* and *S. aureus* (Tables 3, 4). On the other hand (as shown by array data here) the gene expression for DNA and RNA polymerases is not down-regulated by IQ-238, but instead increased (up to almost four times). Our modelling can explain both findings. IQ-238 does not directly affect the DNA and RNA, but rather interferes with the carbohydrate pathways including several enzymes not apparent from the gene expression data.

Utilizing our model, the bacteriostatic effects (Table 2) of IQ-238 on *S. aureus* HG001 were mapped on the two investigated staphylococcal strains, *S. aureus* USA300 and *S. epidermidis* RP62A, and can now be described in detail by its effects on the activity of specific enzymes and pathways, in particular on glycolysis. However, the primary targets of IQ-238 are only mirrored by our methods as far as enzyme activity changes can be measured and detected. In particular, we will do further biochemical follow-up studies (including direct enzyme activity measurements) to determine the direct interactions of this fascinating substance class of IQs.

Both modelled strains are severely affected in their carbohydrate metabolism by IQ-238. As shown, the glycolysis is particularly affected (Tables 3, 4). The gene expression for 6-phosphofructokinase, fructose-bisphosphate-aldolase, and the glyceraldehyde-3-P-dehydrogenase are

down-regulated 3 to 4 fold (Table 1). In combination with metabolic flux modelling the full detail of all effects on the organisms emerges.

Not only enzymes are seen as metabolically changing, which are hampered in their gene expression, but also enzymes which were not affected in their expression level. The latter show a decline in their activity. This is most predominant action in the reaction cascade from fructose-6-phosphate to oxaloacetate in glycolysis. Whereas the gene expression of the first 4 enzymes (see above) is down-regulated, the enzymes phosphoglycerate-kinase, pyruvate-phosphotransferase, 2-phospho-D-glycerate-hydro-lyase, PEP-carboxylase and 2-phospho-D-glycerate-2,3-phosphomutase are not affected in their respective gene expression - still their activitiy is lowered by roughly 50% in both strains (Tables S4, S5, 3, 4).

Effects of secondary metabolites from the compound, like host-pathogen interactions and more complex system effects were not systematically investigated in this work. However, the metabolite measurements show for selected metabolites (UDP-MurNAc-Ala-Glu, UDP-GlcNAc/-GalNAc) of cell wall metabolism a strong accumulation (which is indicative of that these metabolites pile up and cell wall synthesis would thus be blocked). IQ-238 has less systemic effects than IQ-143, since IQ-238 mainly affects carbohydrate metabolism. However, Voronoi treemaps (Fig. 6) by their increased sensitivity show that apart from this strong effect, the isoqinoline IQ-238 has also mild systemic effects although opposite in most cases to that observed for IQ-143. IQ-238 increased the activity of several pathways, including pathways related to stress response (prophage activation for instance; furthermore, and validated here, cell wall metabolism).
However, since first mouse experiments suggest toxicity of IQ-238, this substance should presently only be considered as a lead structure for future drug development. Based on the promising results regarding antibiosis in staphylococci redesign of the compound will exploit accumulated results. One possibility is to form a pro-drug that is not active

in the host but will only be activated after being metabolized in staphylococci.

Improving NIQ lead compounds

Naphthylisoquinolines, derived from the natural compound ancystrocladine found in tropical lianas, may represent a promising class of novel antibiotic leads. We earlier observed some indication to this end examining the lead IQ-143. The present study is an effort to broaden this analysis by including first pharmacological data on IQ-238 treatment and growth inhibition experiments for staphylococci with gene expression analysis of the resulting changes. To evaluate the therapeutic window, mammalian cell culture experiments were considered. A detailed bioinformatical analysis included network modelling and functional cluster analysis as well as Voronoi tessalations. We collected all resulting network effects on different enzymes comparing *Staphylococcus aureus*, *S. epidermidis* and human and murine cells. Note that for the bacteria detailed gene expression and metabolite data were collected, for human and murine cells only toxicity profiles were collected as well as *in silico* modelling done. To broaden the evaluation of this new class of potential antibiotic substances we compared the results for IQ-238 not only to IQ-143 but a number of NIQs for which results are available comparing antibiotic and toxic properties to their chemical properties. This comparison not only shows the therapeutic window for all compounds we investigated so far, but supports the potential of IQ-238 as a lead and delineates better the region of chemical space to explore in the context of alternative NIQs.

Furthermore, by designing a modified IQ-238 as a pro-drug, which is only activated in staphylococci after action of the modification enzyme absent in human, the above antibiotic effects should be transmitted only to the bacteria and the toxic effects are largely kept away from the host. Certainly this theoretical suggestion requires further experimental tests.

Several promising lead NIQ structures with good antibiotic activity against Leishmania and Trypanosomes (see Figure 7) proved to be toxic in mouse macrophages J774.1 cells (Figure 8). IQ-238 with its negative octanol-

water coefficient – but otherwise fulfilling the Lipinksi criterias - had low toxicity (IC_{50} against J774.1 cells reached at more than 100 µM compound) and very good activities against *T. brucei*, *C. albicans*, *S. aureus* and *S. epidermidis* (Table 2). Principle component analysis separates cumulated NIQ data considering antibiotic, as well as cytotoxic potential, compared to principle components of chemical properties. These data can be combined with the above results to suggest directions for further NIQ lead development: Further lead development should focus on IQ-238-like additional changes (derivatization, substitutions) regarding the naphthyl moiety in NIQs. In particular, changing IQ-238 to a more hydrophilic molecule should improve its administration, solubility and prevent neurotoxic side-effects. This substitution is best achieved at the phenolic moiety at the positions not involved in binding to *S. aureus* enzymes of the carbohydrate metabolism as compared to IQ-143 (which does not show such direct effects on *S.aureus* carbohydrate metabolic enzymes).

Conclusions

Our combination of chemical compound properties prediction, PCA, Voronoi tree calculations, metabolic modelling, analysis of enzyme activity, as well as the incorporation of genome-wide transcriptome data directly into the large-scale metabolic models, allowed us to describe in an integrated picture the diverse pathway effects of the antibiotic compound IQ-238 on the metabolism of human pathogens (*S. aureus, S. epidermidis*).

As a requirement for the modelling, the genome sequences were partially re-annotated. Metabolites were measured for validation of the results. The results point out advantageous properties of IQ-238 compared both to alternative NIQs as well as the extensively previously tested IQ-143. Specifically, phenolic side-effects directly acting on the mitochondrial respiratory chain were not found for IQ-238 compared to IQ-143. In contrast, carbohydrate metabolism was broadly regulated down and this with a good therapeutic window compared to the effects observed in human cell culture (toxic concentration for human is above 100 µM for IQ-

238 as tested in cell culture, still higher than 40 µM as observed for IQ-143). Furthermore, we compared both antibiotics in increasing concentrations. In both, there were no resistance mutations detected at lower concentrations, spontaneous resistance development was not observed neither for IQ-238 nor for IQ-143.

The chemical properties from the statistical analysis suggest also that IQ-238 better satisfies Lipinski´s rule of five as the polar surface area is larger and the logP is lower as in IQ-143. This study was devised to obtain an overview on pathway changes and compare different IQs in these effects including metabolite measurements for validation. This is complementary, and in fact, no substitute, to more direct chemical investigations on modification of a primary target. Nevertheless, the pathway effects studied here help, in particular together with the toxicity measurements done on human cells, to identify the most promising lead IQ.

IQ-238 is in an island where a number of promising lead molecules are situated and this can and should now be explored for instance are hydrophilic modifications as outlined above to turn the leads into new antibiotics for clinic and patients. We elucidate at the same time adaptation of pathogenic bacteria to different environments including antibiosis by pinpointing affected pathways. The techniques and their combination are made available for similar efforts in drug development and medical microbiology.

Acknowledgments

Author contributions

AC did the genome re-annotation, chemical properties calculations, and the set up and calculation of the different metabolic models. CL provided R- and PERL- scripts for the statistical evaluation. JB calculated and interpreted Voronoi treemaps. KO did all gene expression analysis experiments and provided infection biology expertise, TM participated in these. PF, JS and AF did array handling and analysis. KD, MS and ML provided metabolic validation measurements and statistical calculations for these. JH tested antibiotic inhibition and resistance development. TAO did all cell toxicity tests. GB, MU, LL, HB and AP provided chemical expertise. HB provided NIQ data. TD led and guided the study, supervised AC, and was involved in the data analysis of all data sets. All authors participated in the writing of the manuscript and approved its final version.

Funding

We thank the German Research Council (Deutsche Forschungsgemeinschaft DFG), grants SFB630 (projects A1, A2, B5, Z1) and TR34 (A8 for CL, TD; Z1 for JB; Z3 for KO; Z4 for KD, ML) and the State of Bavaria (AC, TD) for funding, as well as our colleagues for stimulating discussions.

References

1. Baba, T., Takeuchi, F., Kuroda, M., Yuzawa, H., Aoki, K., Oguchi, A., Nagai, Y., Iwama, N., Asano, K., Naimi, T., Kuroda, H., Cui, L., Yamamoto, K., Hiramatsu, K., 2002. Genome and virulence determinants of high virulence community-acquired MRSA. Lancet. 359(9320):1819-27.
2. Bernhardt, J., Funke, S., Hecker, M., Siebourg, J., 2009. Visualizing gene expression data via Voronoi treemaps. Voronoi Diagrams in Science and Engineering. ISVD '09. 6th International Symposium. 0: 233-241. ISBN: 978-0-7695-3781-8.
3. Bringmann, G., Gulder, T., Hentschel, U., Meyer, F., Moll, H., Morschhäuser, J., Ponte-Sucre, A., Ziebuhr, W., Stich, A., Brun, R., Müller, W.E.G., Mudogo, V., 2007. Preparation of isoquinolines as antibacterial coating materials. PCT/EP2007/008440.
4. Bringmann, G., Gulder, T., Hertlein, B., Hemberger, Y., Meyer, F., 2010. Total Synthesis of the N,C-Coupled Naphthylisoquinoline Alkaloids Ancistrocladinium A and B and Related Analogues. J. Am. Chem. Soc. 132:1151-1158.r
5. Bringmann, G., Gulder, T., Reichert, M., Meyer, F., 2006. Ancisheynine, the First N,C-Coupled Naphthylisoquinoline Alkaloid: Total Synthesis and Stereochemical Analysis. Org. Lett. 8:1037-1040.
6. Bringmann, G., Hertlein-Amslinger, B., Kajahn, I., Dreyer, M., Brun, R., Moll, H., Stich, A., Ioset, NK., Schmitz, W., Ngoc, L.H., 2010. Phenolic analogs of the N,C-coupled naphthylisoquinoline alkaloid ancistrocladinium A, from Ancistrocladus cochinchinensis (Ancistrocladaceae), with improved antiprotozoal activities. Phytochemistry. 72(1):89-93.
7. Bringmann, G., Kajahn, I., Reichert, M., Pedersen, S.H.E., Faber, J.H., Gulder T., Brun, R., Christensen, S.B., Ponte-Sucre, A., Moll, H., Heubl, G., Mudogo, V., 2006. Ancistrocladinium A and B, the First N,C-Coupled Naphthyldihydroisoquinoline Alkaloids, from a Congolese Ancistrocladus Species. J. Org. Chem. 71:9348-9356.

8. Cecil, A., Rikanovic, C., Ohlsen, K., Liang, C., Bernhardt, J., Oelschlaeger, T.A., Gulder, T., Bringmann, G., Holzgrabe, U., Unger, M., Dandekar, T. 2011. modelling antibiotic and cytotoxic effects of the dimeric isoquinoline IQ-143 on metabolism and its regulation in *Staphylococcus aureus*, *Staphylococcus epidermidis* and human cells. Genome Biol. 12(3):R24.
9. Charbonnier, Y., Gettler, B., François, P., Bento, M., Renzoni, A., Vaudaux, P., Schlegel, W., Schrenzel, J., 2005. A generic approach for the design of wholegenome oligoarrays, validated for genomotyping, deletion mapping and gene expression analysis on *Staphylococcus aureus*. BMC Genomics. 6:95.
10. Cheng, A.G., Kim, H.K., Burts, M.L., Krausz, T., Schneewind, O., Missiakas, D.M., 2009. Genetic requirements for Staphylococcus aureus abscess formation and persistence in host tissues. FASEB J. 23:3393-404. {Published online 2009.}
11. Churchill, G.A., 2004. Using ANOVA to analyze microarray data. Biotechniques. 37(2):173-5, 177.
12. Diep, B.A., Gill, S.R., Chang, R.F., Phan, T.H., Chen, J.H., Davidson, M.G., Lin, F., Lin, J., Carleton, H.A., Mongodin, E.F., Sensabaugh, G.F., Perdreau-Remington, F., 2006. Complete genome sequence of USA300, an epidemic clone of community-acquired methicillin-resistant *Staphylococcus aureus*. Lancet. 367:731-9.
13. Dörries K, Lalk M., 2013. Metabolic footprint analysis uncovers strain specific overflow metabolism and D-isoleucine production of Staphylococcus aureus COL and HG001. PLoS One. 8(12):e81500.
14. Dörries K, Schlueter R, Lalk M., 2014. The impact of antibiotics with various target sides on the metabolome of *Staphylococcus aureus*. Antimicrob Agents Chemother. Sep 15. pii: AAC.03104-14. [Epub ahead of print]
15. Fillinger S, Boschi-Muller S, Azza S, Dervyn E, Branlant G, et al., 2000. Two glyceraldehyde-3-phosphate dehydrogenases with opposite physiological roles in a nonphotosynthetic bacterium. J Biol Chem 275: 14031–14037.

16. Gaudermann, P., Vogl, I., Zientz, E., Silva, FJ., Moya, A., Gross, R., Dandekar, T., 2006. Analysis of and function predictions for previously conserved hypothetical or putative proteins in *Blochmannia floridanus*. BMC Microbiology. 6:1.
17. Gentleman, R.C., Ihaka, R., 1996. R: A Language for Data Analysis and Graphics. J. Comp. Graph. Statistics. 5:299-314.
18. Gill, S.R., Fouts, D.E., Archer, G.L., Mongodin, E.F., Deboy, R.T., Ravel, J., Paulsen, I.T., Kolonay, J.F., Brinkac, L., Beanan, M., Dodson, R.J., Daugherty, S.C., Madupu, R., Angiuoli, S.V., Durkin, A.S., Haft, D.H., Vamathevan, J., Khouri, H., Utterback, T., Lee, C., Dimitrov, G., Jiang, L., Qin, H., Weidman, J., Tran, K., Kang, K., Hance, I.R., Nelson, K.E., Fraser, C.M., 2005. Insights on evolution of virulence and resistance from the complete genome analysis of an early methicillin-resistant *Staphylococcus aureus* strain and a biofilm-producing methicillin-resistant *Staphylococcus epidermidis* strain. J. Bacteriol. 187:2426-2438.
19. Grundmann, H., Aanensen, D.M., van den Wijngaard, C.C., Spratt, B.G., Harmsen, D., Friedrich, A.W., and the European Staphylococcal Reference Laboratory Working Group., 2010. Geographic Distribution of Staphylococcus aureus Causing Invasive Infections in Europe: A Molecular-Epidemiological Analysis. PLoS Med. 7:e1000215.
20. Haft, D.H., Selengut, J.D., White, O., 2003. The TIGRFAMs database of protein families. Nucleic acids research 31(1): 371–3.
21. Herbert, S., Ziebandt, A.K., Ohlsen, K., Schäfer, T., Hecker, M., Albrecht, D., Novick, R., Götz, F., 2010. Repair of global regulators in *Staphylococcus aureus* 8325 and comparative analysis with other clinical isolates. Infect. Immun. 78:2877-2889.
22. Holden, M.T., Feil, E.J., Lindsay, J.A., Peacock, S.J., Day, N.P., Enright, M.C., Foster, T.J., Moore, C.E., Hurst, L., Atkin, R., Barron, A., Bason, N., Bentley, S.D., Chillingworth, C., Chillingworth, T., Churcher, C., Clark, L., Corton, C., Cronin, A., Doggett, J., Dowd, L., Feltwell, T., Hance, Z., Harris, B., Hauser, H., Holroyd, S., Jagels, K., James, K.D., Lennard, N., Line, A., Mayes, R., Moule,

S., Mungall, K., Ormond, D., Quail, M.A., Rabbinowitsch, E., Rutherford, K., Sanders, M., Sharp, S., Simmonds, M., Stevens, K., Whitehead, S., Barrell, B.G., Spratt, B.G., Parkhill, J., 2004. Complete genomes of two clinical *Staphylococcus aureus* strains: evidence for the rapid evolution of virulence and drug resistance. Proc. Natl. Acad. Sci. USA. 101(26):9786-91. {Epub 2004 Jun 22.}

23. Kanehisa, M., Araki, M., Goto, S., Hattori, M., Hirakawa, M., Itoh, M., Katayama, T., Kawashima, S., Okuda, S., Tokimatsu, T., Yamanishi, Y., 2008. KEGG for linking genomes to life and the environment. Nucleic Acids Res. 36:D480-D484.
24. Kuroda, M., Ohta, T., Uchiyama, I., Baba, T., Yuzawa, H., Kobayashi, I., Cui, L., Oguchi, A., Aoki, K., Nagai, Y., Lian, J., Ito, T., Kanamori, M., Matsumaru, H., Maruyama, A., Murakami, H., Hosoyama, A., Mizutani-Ui, Y., Takahashi, N.K., Sawano, T., Inoue, R., Kaito, C., Sekimizu, K., Hirakawa, H., Kuhara, S., Goto, S., Yabuzaki, J., Kanehisa, M., Yamashita, A., Oshima, K., Furuya, K., Yoshino, C., Shiba, T., Hattori, M., Ogasawara, N., Hayashi, H., Hiramatsu, K., 2001. Whole genome sequencing of meticillin-resistant *Staphylococcus aureus*. Lancet. 357(9264):1225-40.
25. Mattner, F., Biertz, F., Ziesing, S., Gastmeier, P., Chaberny, I.F., 2010. Long-term persistence of MRSA in re-admitted patients. Infection. 38:363-371. {Published online 2010.}
26. Oksanen, J., Blanchet, F.G., Kindt, R., Legendre, P., Minchin, P.R., O'Hara, R.B., Simpson, G.L., Solymos, P., Stevens, M.H.M., Wagner, H., 2010. vegan: Community Ecology Package. R package version 2.1-9/r2044.
27. Otto, A., Bernhardt, J., Herbst, F.A., Siebourg, J., Mäder, U., Hecker, M., Becher, D., 2010. System-wide temporal profiling of proteins in glucose starved *Bacillus subtilis*. Nat. Commun. 1:137
28. Pimentel-Elardo, S.M., Kozytska, S., Bugni, T.S., Ireland, C.M., Moll, H., Hentschel, U., 2010. Anti-parasitic compounds from Streptomyces sp. strains isolated from Mediteranean sponges. Mar. Drugs. 8:373-380.
29. Ponte-Sucre, A., Faber, J.H., Gulder, T., Kajahn, I., Pedersen,

S.E.H., Schultheis, M., Bringmann, G., Moll, H., 2007. Activities of Naphthylisoquinoline Alkaloids and Synthetic Analogs against Leishmania major. Antimicrob. Agents Chemother. 51:188-194.

30. Ponte-Sucre, A., Gulder, T., Gulder, A.M., Vollmers, G., Bringmann, G., Moll, H., 2010. Alterations on the Structure of *Leishmania major* induced by N-Arylisoquinolines correlate with Compound Accumulation and Disposition. J. Med. Microbiol. 59:69-75.
31. Ponte-Sucre, A., Gulder, T., Wegehaupt, A., Albert, C., Rikanovic, C., Schaeflein, L., Frank, A., Schultheis, M., Unger, M., Holzgrabe, U., Bringmann, G., Moll, H., 2009. Structure-Activity Relationship and Studies on the Molecular Mechanism of Leishmanicidal N,C-Coupled Arylisoquinolinium Salts. J. Med. Chem. 52:626-636.
32. Price, M.N., Huang, K.H., Alm, E.J., Arkin, A.P. 2005. A Novel Method for Accurate Operon Predictions in All Sequenced Prokaryotes. Nucleic Acids Research. 33:880-892.
33. Price, M.N., Alm, E.J., Arkin, A.P., 2005. Interruptions in gene expression drive highly expressed operons to the leading strand of DNA replication..Nucleic Acids Research. 33:3224-3234.
34. Renzoni, A., Barras, C., François, P., Charbonnier, Y., Huggler, E., Garzoni, C., Kelley, W.L., Majcherczyk, P., Schrenzel, J., Lew, D.P., Vaudaux, P., 2006. Transcriptomic and functional analysis of an autolysis-deficient, teicoplanin-resistant derivative of methicillin-resistant *Staphylococcus aureus*. Antimicrob. Agents. Chemother. 50(9):3048-61.
35. Scherl, A., François, P., Charbonnier, Y., Deshusses, J.M., Koessler, T., Huyghe, A., Bento, M., Stahl-Zeng, J., Fischer, A., Masselot, A., Vaezzadeh, A., Gallé, F., Renzoni, A., Vaudaux, P., Lew, D., Zimmermann-Ivol, C.G., Binz, P.A., Sanchez, J.C., Hochstrasser, D.F., Schrenzel, J., 2006. Exploring glycopeptide-resistance in *Staphylococcus aureus*: a combined proteomics and transcriptomics approach for the identification of resistance-related markers. BMC Genomics. 7:296.
36. Schuster, S., Fell, D.A., Dandekar, T., 2000. A general definition of metabolic pathways useful for systematic organization and analysis

of complex metabolic networks. Nature Biotech. 18:326-332.

37. Schwarz, R., Liang, C., Kaleta, C., Kühnel, M., Hoffmann, E., Kuznetsov, S., Hecker, M., Griffiths, G., Schuster, S., Dandekar, T., 2007. Integrated network reconstruction, visualization and analysis using YANAsquare. BMC Bioinformatics. 8:313.
38. Schwarz, R., Musch, P., von Kamp, A., Engels, B., Schirmer, H., Schuster, S., Dandekar, T., 2005. YANA - a software tool for analyzing flux modes, gene-expression and enzyme activities. BMC Bioinformatics. 6:135. {Published online 2005.}
39. Uchiyama, I., 2003. MBGD: microbial genome database for comparative analysis. Nucleic Acids Res. 31:58-62
40. Uchiyama, I., 2007. MBGD: a platform for microbial comparative genomics based on the automated construction of orthologous groups. Nucleic Acids Res. 35:D343-D346
41. Uchiyama, I., Higuchi, T., Kawai, M., 2010. MBGD update 2010: toward a comprehensive resource for exploring microbial genome diversity. Nucleic Acids Res. 38:D361-D365
42. Wright, J.A., Nair, S.P., 2010. Interaction of staphylococci with bone. Int. J. Med. Microbiol. 300:193-204.
43. Yang, L.K., Glover, R.P., Yoganathan, K., Sarnaik, J.P., Godbole, A.J., Soejarto, D.D., Buss, A.D., Butler, M.S., 2003. Ancisheynine, a novel naphthylisoquinolinium alkaloid from Ancistrocladus heyneanus. Tetrahedron Lett. 44:5827-5829.
44. Zirkel, J., Cecil, A., Schäfer, F., Rahlfs, S., Ouedraogo, A., Xiao, K., Sawagogo, S., Coulibaly, B., Becker, K., Dandekar, T., 2012. Analyzing thiol- dependent redox networks in the presence of methyleneblue and other anti- malarial agents with RT-PCR-supported in silico modelling. Bioinform Biol Insights. 6:287-302

Table 1. Key gene expression changes in *S. aureus* after administration of IQ-238[1]

EC- number	**Enzyme description**	**gene**	**fold- change**
2.3.3.1	citrate synthase	***citZ***	-3,038
2.A.15	choline transporter	***cudT***	14,333
2.4.2.1	purine nucleoside phosphorylase	***deoD***	-3,737
4.1.2.13	fructose-bisphosphate aldolase	***fbaA***	-4,327
3.1.3.11	fructose-bisphosphatase	***fbp***	-3,643
1.2.7.3	ferredoxin	***fer***	6,045
4.2.1.2	fumarate hydratase	***fumC***	-9,527
1.2.1.12	glyceraldehyde 3-phosphate dehydrogenase 2 NAD+	***gapB***	-2,995
1.2.1.13	glyceraldehyde 3-phosphate dehydrogenase 2 NADP+	***gapB***	-2,995
1.2.4.1	pyruvate dehydrogenase E1 component alpha subunit	**pdhA**	-3,541
2.4.2.2	pyrimidine-nucleoside phosphorylase	**pdp**	-4,675
2.7.1.11	6-phosphofructokinase	**pfkA**	-3,535
5.3.1.9	glucose-6-phosphate isomerase	**pgi**	-4,411
2.7.7.7	DNA polymerase III PolC	**polC**	3,716
4.3.2.2.	adenylosuccinate lyase	**purB**	-3,218
6.3.5.3	phosphoribosylformylglycinamidine synthase II	**purL**	-3,521
6.4.1.1.	pyruvate carboxylase	**pycA**	-3,010
2.4.2.10	orotate phosphoribosyltransferase	**pyrE**	-6,600
4.1.1.23	orotidine 5'-phosphate decarboxylase	**pyrF**	-5,772
2.7.7.6	DNA-directed RNA polymerase subunit beta	**rpoB**	4,192
2.7.7.6	DNA-directed RNA polymerase subunit delta	**rpoE**	3,025
1.1.1.27	L-lactate dehydrogenase	**SA2395**	-9,532
1.1.1.1	alcohol dehydrogenase, zinc-containing	**SACOL0237**	-6,022
SERP1944	EmrB/QacA family drug resistance transporter	**SACOL2413**	3,637
2.7.1.48	uridine kinase	**udk**	3,730
2.4.2.22	xanthine phosphoribosyltransferase	**xprT**	4,160

[1]The fold changes given in this table were used to fit the gene expression changes directly to the enzyme activities in our models.

Table 2. Activities of IQ-238 against pathogens[1]

IQ-238	**MIC** [µM]	**IC50** [µM]	**[%]**	**IQ-143**	**MIC** [µM]	**IC50** [µM]	**[%]**
S. aureus	2,5			*S.* aureus	5		
S. epidermidis	0,16			*S.* epidermidis	0,63		
E. coli	40			*E.* coli	20		
P. aeruginosa	>160			*P.* aeruginosa	>160		
C. albicans	5			*C.* albicans	1,25		
293T		58,1		293T		42,4	
T. brucei		0,27		*T.* brucei		0,06	
L. major		19,6		*L.* major		23,57	
J774.1		>100		J774.1		40,15	
Inhibition of biofilm formation			95	Inhibition of biofilm formation			100
Growth inhibition			95	Growth inhibition			95

[1]The data shown here are the activities of IQ-143 and IQ238 against different pathogens as well as human cell lines according to toxicity testing.

Table 3. Enzyme activities after administration of IQ-238 in *S. epidermidis* RP62A[1]

	IQ-238 NOT ADDED	IQ-238 ADDED	*S. epidermidis*	*S. epidermidis*
Enzyme name	Normalized flux	Normalized flux	Difference enzyme activity	% Remaining activity
"Glyc_fructose-bisphosphatase"	0.0479	0.0029	-0.045	0.061
"Glyc_6-phosphofructokinase"	0.1275	0.0464	-0.081	0.364
"Glyc_fructose-bisphosphat-aldolase"	0.0796	0.0435	-0.036	0.546
"Glyc_glyceraldehyde-3-P-dehydrogenase_NAD+"	0.0317	0.0144	-0.017	0.454
"Glyc_glyceraldehyde-3-P-dehydrogenase_NADP+"	0.1275	0.0726	-0.055	0.569
"Glyc_phosphoglycerate-kinase"	-0.1592	-0.0870	0.072	0.546
"Glyc_2-Phospho-D-glycerate-2.3-phosphomutase"	-0.1592	-0.0870	0.072	0.546
"Glyc_2-phospho-D-glycerate-hydro-lyase"	0.1592	0.0870	-0.072	0.546
"PurM_pyruvate-phosphotransferase_ATP"	0.0000	0.0000	0.000	0.000
"PurM_pyruvate-phosphotransferase_dATP"	0.0160	0.0110	-0.005	0.688
"PurM_pyruvate-phosphotransferase_dGTP"	0.0160	0.0110	-0.005	0.688
"TCA_PEP-carboxylase"	-0.2073	-0.1199	0.087	0.578

[1]Given here are the calculated enzyme activities after administration of IQ-238 in a sublethal dose.

Table 4. Enzyme activities after administration of IQ-238 in *S. aureus* USA300[1]

Enzyme name	IQ-238 NOT ADDE Normalized flux	IQ-238 ADDED Normalized flux	*S. aureus* Difference enzyme activity	*S. aureus* % Remaining activity
"Glyc_fructose-bisphosphatase"	0.0356	0.0029	-0.033	0.081
"Glyc_6-phosphofructokinase"	0.1526	0.0763	-0.076	0.500
"Glyc_fructose-bisphosphat-aldolase"	0.1169	0.0734	-0.044	0.628
"Glyc_glyceraldehyde-3-P-dehydrogenase_NAD+"	0.0304	0.0129	-0.018	0.424
"Glyc_glyceraldehyde-3-P-dehydrogenase_NADP+"	0.2034	0.1339	-0.070	0.658
"Glyc_phosphoglycerate-kinase"	-0.2339	-0.1468	0.087	0.628
"Glyc_2-Phospho-D-glycerate-2.3-phosphomutase"	-0.2339	-0.1468	0.087	0.628
"Glyc_2-phospho-D-glycerate-hydro-lyase"	0.2339	0.1468	-0.087	0.628
"PurM_pyruvate-phosphotransferase_ATP"	0.0000	0.0103	0.010	0.000
"PurM_pyruvate-phosphotransferase_dATP"	0.0102	0.0103	0.000	1.010
"PurM_pyruvate-phosphotransferase_dGTP"	0.0102	0.0103	0.000	1.010
"TCA_PEP-carboxylase"	-0.2645	-0.1777	0.087	0.672

[1]Given here are the calculated enzyme activities after administration of IQ-238 in a sublethal dose.

Table 5. Chemical properties of a selection of naphthylisoquinolines[1]

IQ number:	Atom Count:	Ring Count:	Polar surface Area:	Molecular Weight:	logP:	H bond donor Count:	H bond acceptor Count:	Lipinski rule of 5 Acceptable?	IC50 J774.1 Cells
251	61	4	65,07	435,51	3,90	0,00	6,00	yes	100,00
265	62	4	36,92	430,54	6,52	0,00	4,00	no	35,90
268	52	4	13,11	428,42	1,00	0,00	1,00	yes	100,00
269	20	1	40,46	138,16	2,39	2,00	2,00	yes	100,00
274	41	1	57,53	262,34	4,27	2,00	3,00	yes	32,80
275	36	1	46,53	246,30	4,42	1,00	3,00	yes	27,00
276	40	1	55,76	276,33	4,48	1,00	4,00	yes	29,20
277	46	2	46,53	322,40	5,14	1,00	3,00	no	32,00
278	47	1	52,60	314,44	2,39	0,00	4,00	yes	3,50
279	26	1	63,60	196,20	0,55	1,00	4,00	yes	4,10
281	29	1	52,60	210,23	0,97	0,00	3,00	yes	100,00
283	39	1	49,69	238,32	3,53	2,00	3,00	yes	100,00
285	40	1	46,53	250,33	2,65	1,00	3,00	yes	7,50
299	37	3	3,88	248,34	0,69	0,00	0,00	yes	100,00
300	35	2	13,11	228,31	-0,46	0,00	1,00	yes	100,00
303	45	3	22,34	308,39	0,37	0,00	2,00	yes	20,00
304	51	3	22,34	336,45	1,10	0,00	2,00	yes	5,90
309	43	2	3,88	254,39	1,24	0,00	0,00	yes	100,00
310	49	2	3,88	282,44	2,19	0,00	0,00	yes	100,00
312	48	3	22.34	322,42	1,07	0,00	2,00	yes	17,60
314	63	4	51,80	517,49	0,90	1,00	4,00	no	1,00
324	56	6	39,18	420,50	6,38	1,00	2,00	no	100,00
334	31	2	3,88	277,18	0,47	0,00	0,00	yes	100,00
335	57	4	22,34	390,49	2,09	0,00	2,00	yes	2,90
336	51	4	22,34	358,45	1,55	0,00	2,00	yes	3,77
339	69	7	62,46	539,56	8,41	0,00	4,00	no	100,00
353	55	5	22,34	406,50	2,75	0,00	2,00	yes	2,47
356	44	4	13,11	314,40	1,00	0,00	1,00	yes	26,00
361	20	1	40,46	138,16	2,39	2,00	2,00	yes	35,10
370	18	1	60,60	140,14	0,60	3,00	3,00	yes	78,50
238	86	6	73,78	629,74	-1,17	1,00	5,00	no	100,00
143	82	6	44,68	586,72	-0,61	0,00	4,00	no	40,15

[1]Shown here are the chemical properties as calculated by the MarvinSketch- program from ChemAxon (Marvin Version 5.5.1.0, ChemAxon, Záhony u. 7, Building HX, 1031 Budapest, Hungary. [http://www.chemaxon.com].

Table 6. Metabolite measurements[1]

Metabolite measurement	(FC stress t1/t0) /(FC ctrl t1/t0)	(FC stress t2/t0) / (FC ctrl t2/t0)
trehalose-6-P	14,70	38,55
isocitrate	2,26	1,97
fumarate	1,96	3,01
erythrose-4-P	0,47	2,49
ribulose-5-P	3,63	2,89
sedoheptulose-1.7-bisP*	35,19	52,55
PRPP	1,62	0,04
ATP	0,80	0,54
GMP	4,59	14,05
GDP	4,65	6,32
GTP	5,36	3,55
UTP	4,06	1,98
CMP	5,26	8,37
CDP	7,63	8,81
CTP	8,28	4,97
dCMP	0,54	1,19
FAD	0,56	0,37
NADP+	1,90	1,70
glutamine	7,03	5,23
glutamate	2,26	1,06
homoserine	0,76	0,28
UDP-GlcNAc/-GalNAc	27,87	2,19
UDP-MurNAc-Ala-Glu	6,04	2,30
alanine-alanine	2,04	1,16
CDP-glycerol	3,85	3,54
CDP-ribitol	3,60	6,02

t-test	(FC stress t1/t0) /(FC ctrl t1/t0)	(FC stress t2/t0) /(FC ctrl t2/t0)
trehalose-6-P	0,002	0,022
isocitrate	0,000	0,293
fumarate	0,004	0,000
erythrose-4-P	0,009	0,108
ribulose-5-P	0,009	0,057
sedoheptulose-1.7-bisP*	0,006	0,031
PRPP	0,209	0,003
ATP	0,225	0,001
GMP	0,064	0,000
GDP	0,001	0,026
GTP	0,000	0,002
UTP	0,001	0,011
CMP	0,012	0,001
CDP	0,004	0,024
CTP	0,000	0,001
dCMP	0,003	0,809
FAD	0,000	0,000
NADP+	0,014	0,001
glutamine	0,001	0,003
glutamate	0,002	0,627
homoserine	0,172	0,004
UDP-GlcNAc/-GalNAc	0,005	0,169
UDP-MurNAc-Ala-Glu	0,001	0,068
alanine-alanine	0,010	0,409
CDP-glycerol	0,000	0,000
CDP-ribitol	0,000	0,000

[1]Given here are the metabolite measurements performed to validate the *in silico* calculations comparing controls with IQ-238 administered *S. aureus* HG001 cells. Values of above 1 show accumulation of metabolites, values below one show diminishing metabolite quantities in IQ-238 treated cells compared to unstressed cells. A t-test was also performed. Light red depicts significance at $p < 0.05$, dark red significance at $p < 0.01$.

Table 7. *In silico* fluxes of oxidative phosphorylation[1]

	S. epidermidis				**S. aureus**			
Name	No IQ-238 norm. Flux	IQ-238 added norm. flux	Total difference	% remaining activity	No IQ-238 norm. Flux	IQ-238 added norm. flux	Total difference	% remaining activity
OP_complex1	0,0385	0,0217	-0,017	0,564	0,0327	0,0199	-0,013	0,609
OP_complex2	0,0268	0,014	-0,013	0,528	0,0292	0,0129	-0,016	0,442
OP_complex3	0,0650	0,0357	-0,029	0,549	0,0619	0,0328	-0,029	0,53
OP_complex4	0,0517	0,0287	-0,023	0,555	0,0473	0,0264	-0,021	0,558
OP_complex5	0,0818	0,0478	-0,034	0,584	0,0562	0,0441	-0,012	0,785

[1]This table shows the differences in calculated metabolic flux through the oxidative phosphorylation (complexes 1 to 5) before and after administration of IQ-238. Given are the total flux changes as well as the remaining percentage of activities.

Figure legends

Figure 1. Chemical structure of IQ-238 and IQ-143:
IQ-238 and IQ-143 are different synthetic analogs of the novel-type *N*,*C*-coupled NIQ alkaloid ancisheynine.

Figure 2. Simplified view on the metabolic chart for *S. aureus* and *S. epidermidis*, focussing on central metabolic pathways of interest:
This flow chart illustrates which pathways of the primary metabolism are incorporated into our models. Note that the secondary metabolism is not a part of our model.
An asterisk denotes measurements of metabolites. The measured metabolites are as follows: trehalose-6-P, isocitrate, fumarate, erythrose-4-P, ribulose-5-P, PRPP, ATP, GMP, GDP, GTP, UTP, CMP, CDP, CTP, dCMP, FAD, NADP+, glutamine, glutamate, homoserine, UDP-GlcNAc/-GalNAc, UDP-MurNAc-Ala-Glu, alanine-alanine, CDP-glycerol, CDP-ribitol and sedoheptulose-1.7-bisP.

Figure 3. Changes indicated by metabolic modelling of *S. epidermidis* and *S. aureus:*
Enzyme activity bar plots are given for *S. aureus* and *S. epidermidis:* enzymes highlighted in yellow are specific for IQ-143, enzymes highlighted in blue are specific for IQ-238, whereas enzymes highlighted in green are affected by both compounds.
Many differences are apparent applying metabolic modelling, a stippled box in the diagram and brackets around the enzyme name highlight those enzymes in which the different gene expression values already indicate a significant change after administration of IQ-143.

Figure 4. Voronoi diagram: IQ-143 – 2 x MIC:
This Voronoi tree shows the changes after administration of a 2x minimal inhibitory concentration of IQ-143 on *S.epidermidis*. Pathways given in light-blue background are down-regulated, pathways in brownish colors are up-regulated. Maximum fold changes are given as numbers in the color bar given at the bottom.

Figure 5. Voronoi diagram: IQ-143 – ¼ x MIC:

This Voronoi- tree shows the changes after administration of a 1/4x minimal inhibitory concentration of IQ-143 on *S.epidermidis*. Pathways given in light-blue background are down-regulated, pathways in brownish colors are up-regulated. Maximum fold changes are given as numbers in the color bar given at the bottom.

Figure 6. Voronoi diagram: IQ-238 – 10 x MIC:

This Voronoi- tree shows the changes after administration of a 10x minimal inhibitory concentration of IQ-238 on *S.aureus*. Pathways given in light-blue background are down-regulated, pathways in brownish colors are up-regulated. Maximum fold changes are given as numbers in the color bar given at the bottom.

Figure 7. PCA biological properties of a selection of NIQ compounds:

Shown are the different antibiotic activities of a selection of NIQ compounds (shown in **Table 5**) dependent on their chemical properties. IQ-143 and IQ-238 are located on the left-hand side of the figure. The color coding of the organisms shows the compounds affecting the organism the most: black= no effects detected; yellow= effective against *Y. Pestis;* orange= effective against Trypanosomes and bactericidal, but also toxic to human cells; purple= effective against Trypanosomes, but also toxic to human cells; green= effective against Leishmania, but also toxic; red= effective against Kinetoplastida; blue= effective against Kinetoplastida, but again toxic to human cells.

It should be noted, however, that not all good candidates will be located in this particular area.

Figure 8. PCA toxicity of NIQs:

This PCA shows the chemical properties of a selection of NIQ compounds (shown in Table 5) and their toxicity against mammalian cells. The IC_{50}- values against J774.1 macrophages are given by following color code: light red = IC50 reached at 0 to 20 µM of added compound; dark red= IC50 reached at 21 to 40µM of added compound; black= IC_{50} reached at 41 to 60 µM of added compound; dark green= IC_{50} reached at 61 to 80 µM of added compound; light green= IC_{50} reached at 81 to 100 µM of added compound.

A IQ-238

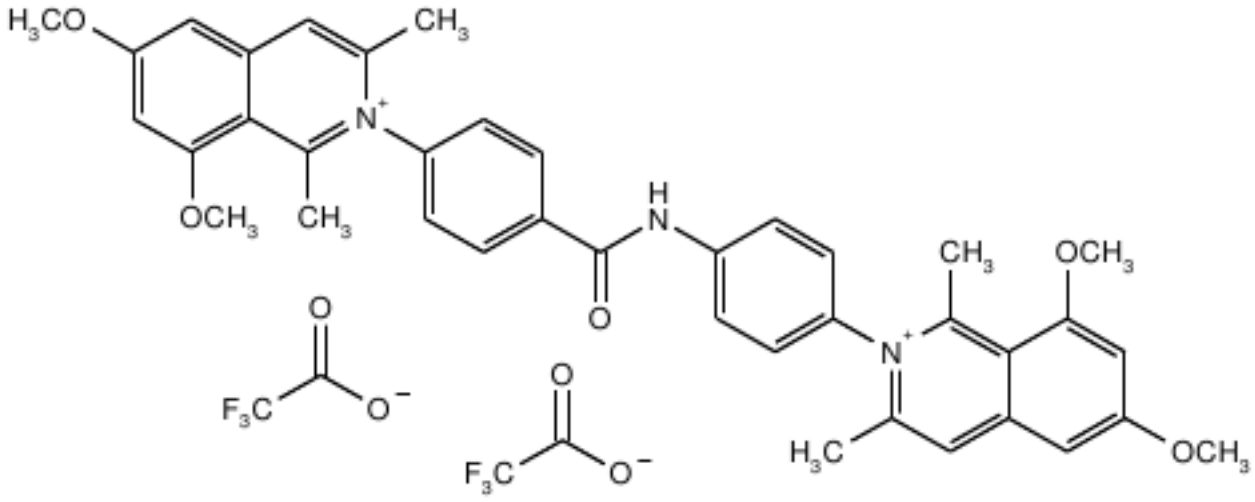

B IQ-143

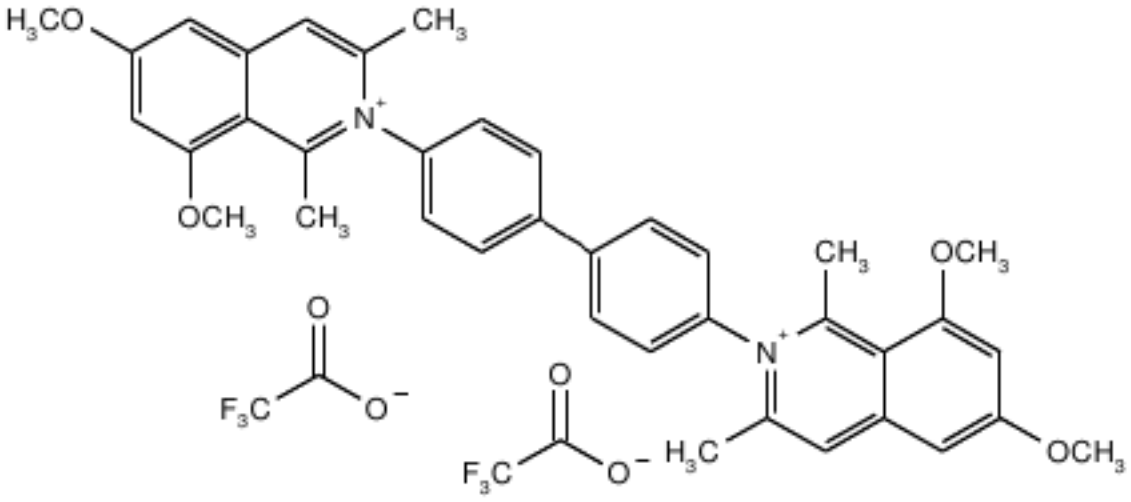

Fig. 1

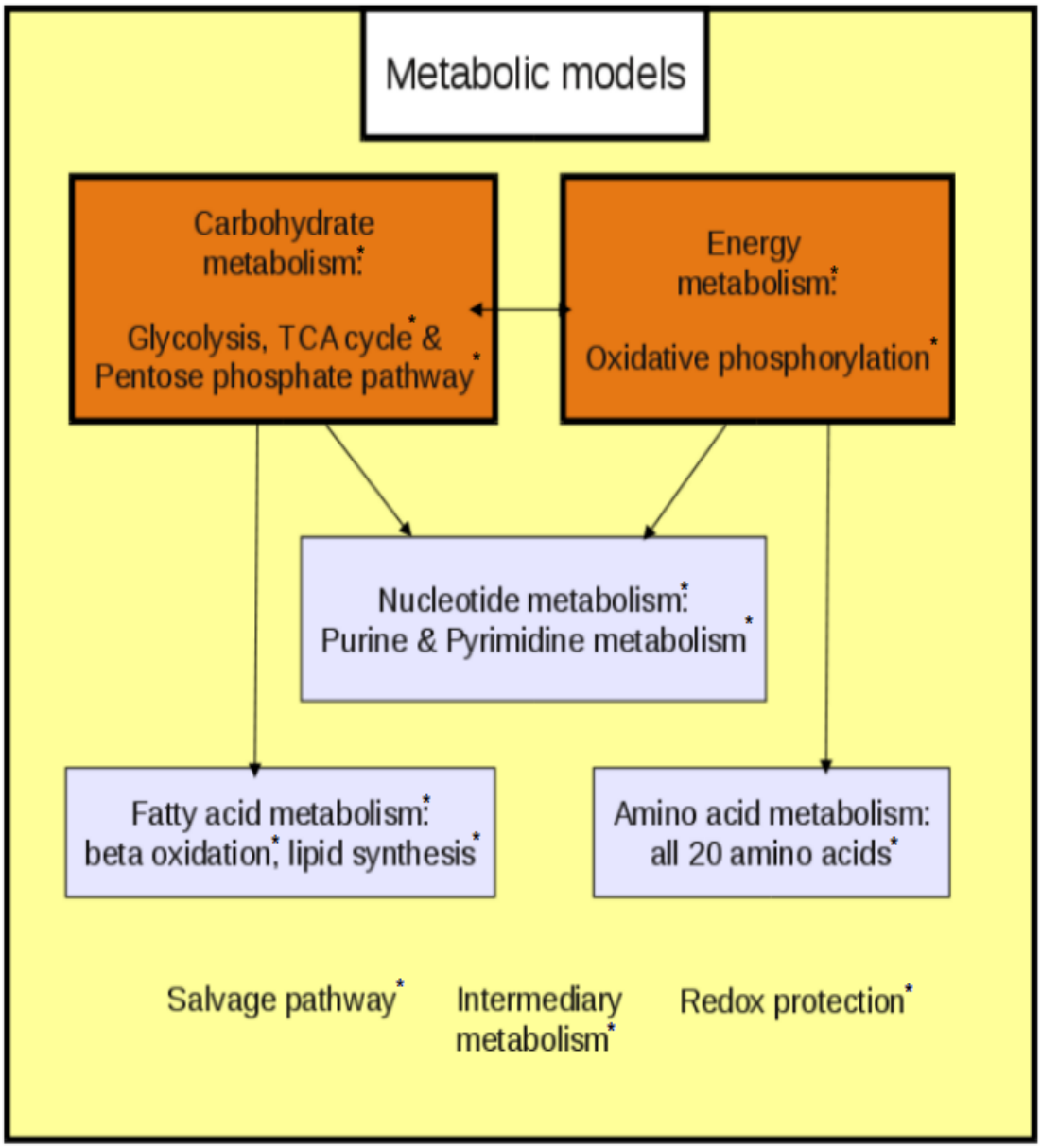
Metabolic models
Carbohydrate metabolism*:
Glycolysis, TCA cycle* & Pentose phosphate pathway*
Energy metabolism*:
Oxidative phosphorylation*
Nucleotide metabolism*:
Purine & Pyrimidine metabolism*
Fatty acid metabolism*:
beta oxidation*, lipid synthesis*
Amino acid metabolism:
all 20 amino acids*
Salvage pathway*
Intermediary metabolism*
Redox protection*

Fig. 2

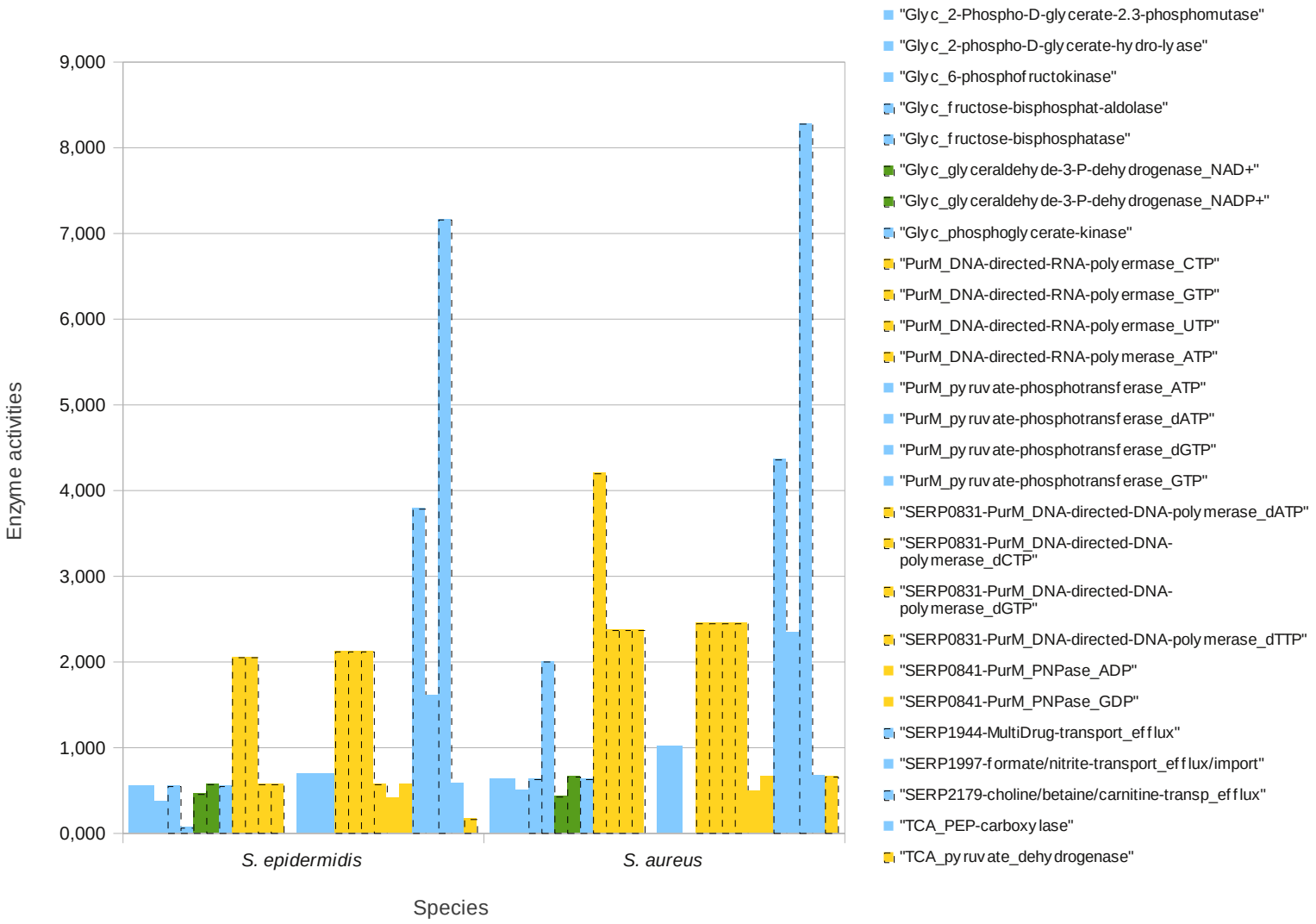
9,000
8,000
7,000
6,000
5,000
4,000
3,000
2,000
1,000
0,000
Enzyme activities
S. epidermidis
S. aureus
Species
"Glyc_2-Phospho-D-glycerate-2.3-phosphomutase"
"Glyc_2-phospho-D-glycerate-hydro-lyase"
"Glyc_6-phosphofructokinase"
"Glyc_fructose-bisphosphat-aldolase"
"Glyc_fructose-bisphosphatase"
"Glyc_glyceraldehyde-3-P-dehydrogenase_NAD+"
"Glyc_glyceraldehyde-3-P-dehydrogenase_NADP+"
"Glyc_phosphoglycerate-kinase"
"PurM_DNA-directed-RNA-polymerase_CTP"
"PurM_DNA-directed-RNA-polymerase_GTP"
"PurM_DNA-directed-RNA-polymerase_UTP"
"PurM_DNA-directed-RNA-polymerase_ATP"
"PurM_pyruvate-phosphotransferase_ATP"
"PurM_pyruvate-phosphotransferase_dATP"
"PurM_pyruvate-phosphotransferase_dGTP"
"PurM_pyruvate-phosphotransferase_GTP"
"SERP0831-PurM_DNA-directed-DNA-polymerase_dATP"
"SERP0831-PurM_DNA-directed-DNA-polymerase_dCTP"
"SERP0831-PurM_DNA-directed-DNA-polymerase_dGTP"
"SERP0831-PurM_DNA-directed-DNA-polymerase_dTTP"
"SERP0841-PurM_PNPase_ADP"
"SERP0841-PurM_PNPase_GDP"
"SERP1944-MultiDrug-transport_efflux"
"SERP1997-formate/nitrite-transport_efflux/import"
"SERP2179-choline/betaine/carnitine-transp_efflux"
"TCA_PEP-carboxylase"
"TCA_pyruvate_dehydrogenase"

Fig. 3

Fig. 4

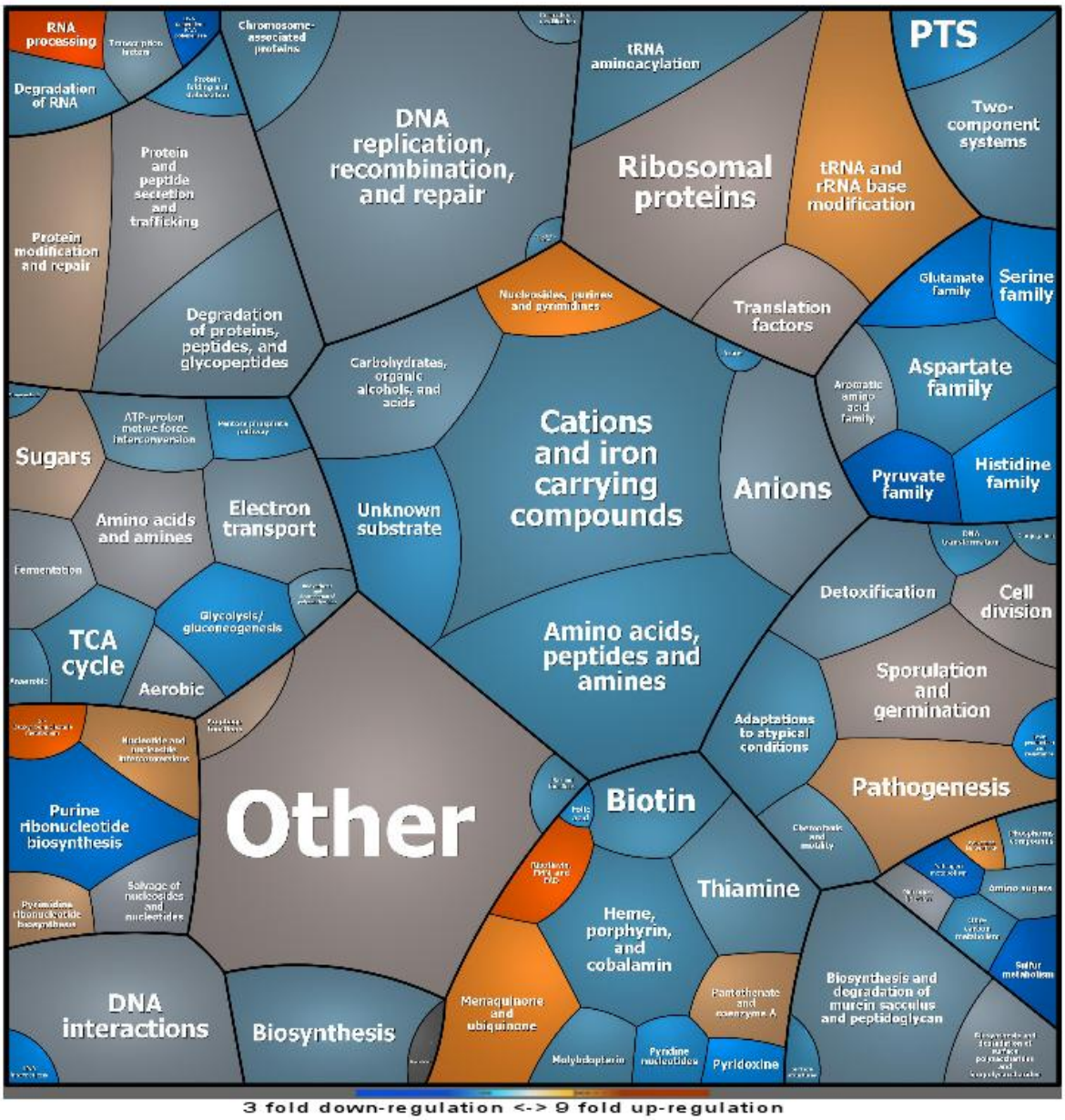
RNA processing
Degradation of RNA
Chromosome-associated proteins
DNA replication, recombination, and repair
tRNA aminoacylation
Ribosomal proteins
tRNA and rRNA base modification
PTS
Two-component systems
Protein and peptide secretion and trafficking
Protein modification and repair
Degradation of proteins, peptides, and glycopeptides
Nucleosides, purines and pyrimidines
Translation factors
Glutamate family
Serine family
Aspartate family
Aromatic amino acid family
Carbohydrates, organic alcohols, and acids
Cations and iron carrying compounds
Anions
Pyruvate family
Histidine family
Sugars
ATP-proton motive force interconversion
Amino acids and amines
Electron transport
Unknown substrate
Fermentation
Glycolysis/ gluconeogenesis
TCA cycle
Aerobic
Amino acids, peptides and amines
Detoxification
Cell division
Sporulation and germination
Adaptations to atypical conditions
Pathogenesis
Other
Biotin
Purine ribonucleotide biosynthesis
Salvage of nucleosides and nucleotides
Thiamine
Heme, porphyrin, and cobalamin
Amino sugars
Sulfur metabolism
Biosynthesis and degradation of murein sacculus and peptidoglycan
DNA interactions
Biosynthesis
Menaquinone and ubiquinone
Pantothenate and coenzyme A
Molybdopterin
Pyridine nucleotides
Pyridoxine
3 fold down-regulation <-> 9 fold up-regulation

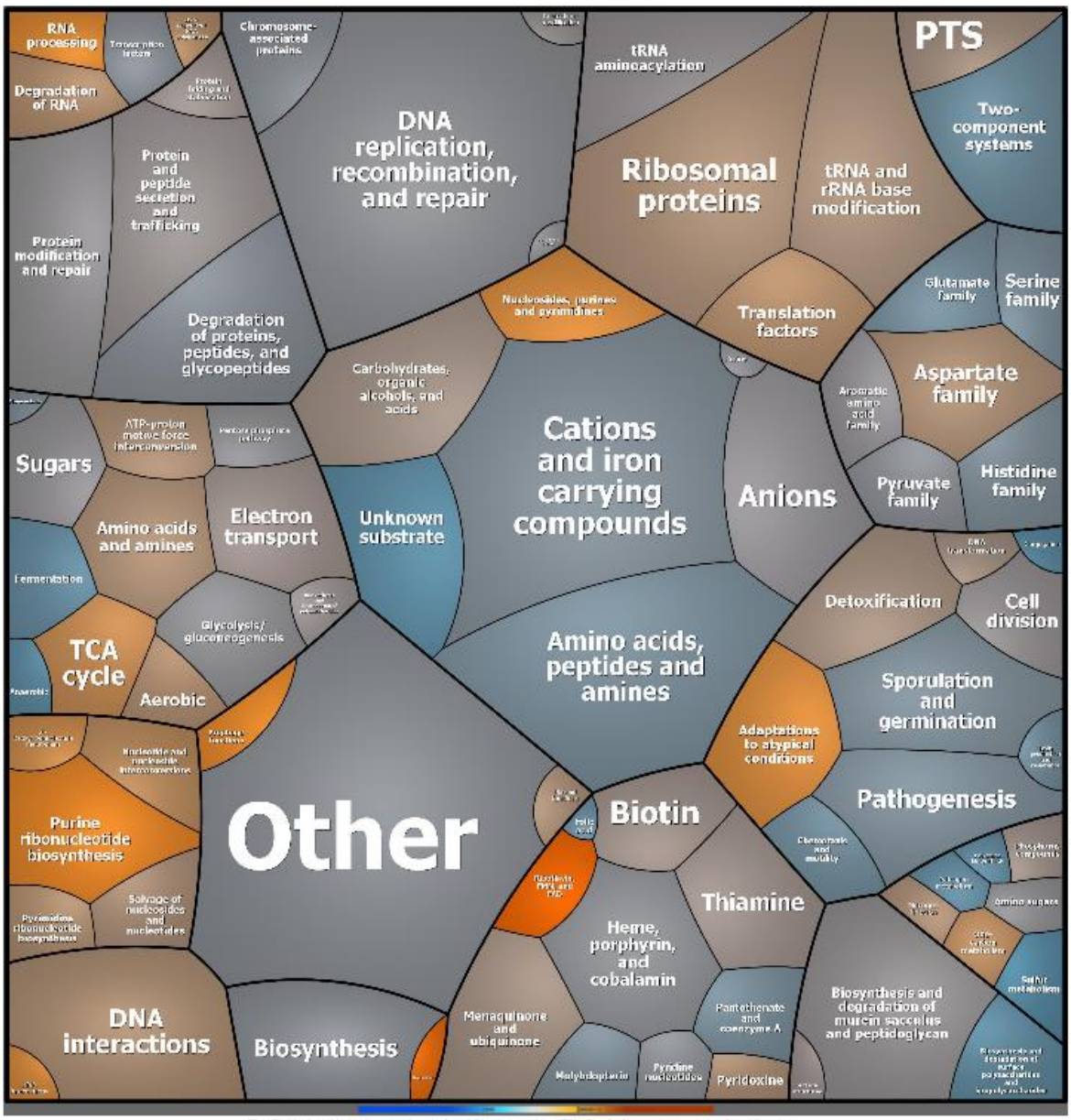
RNA processing
Degradation of RNA
Chromosome-associated proteins
DNA replication, recombination, and repair
tRNA aminoacylation
Ribosomal proteins
tRNA and rRNA base modification
PTS
Two-component systems
Protein and peptide secretion and trafficking
Protein modification and repair
Degradation of proteins, peptides, and glycopeptides
Nucleosides, purines and pyrimidines
Translation factors
Glutamate family
Serine family
Aspartate family
Carbohydrates, organic alcohols, and acids
Cations and iron carrying compounds
Anions
Aromatic amino acid family
Pyruvate family
Histidine family
Sugars
ATP-proton motive force interconversion
Electron transport
Unknown substrate
Amino acids and amines
Fermentation
Glycolysis/ gluconeogenesis
TCA cycle
Aerobic
Amino acids, peptides and amines
Detoxification
Cell division
Sporulation and germination
Adaptations to atypical conditions
Pathogenesis
Other
Biotin
Purine ribonucleotide biosynthesis
Salvage of nucleosides and nucleotides
Thiamine
Heme, porphyrin, and cobalamin
DNA interactions
Biosynthesis
Menaquinone and ubiquinone
Pantothenate and coenzyme A
Biosynthesis and degradation of murein sacculus and peptidoglycan
Pyridoxine
3 fold down-regulation <-> 7 fold up-regulation

Fig. 5

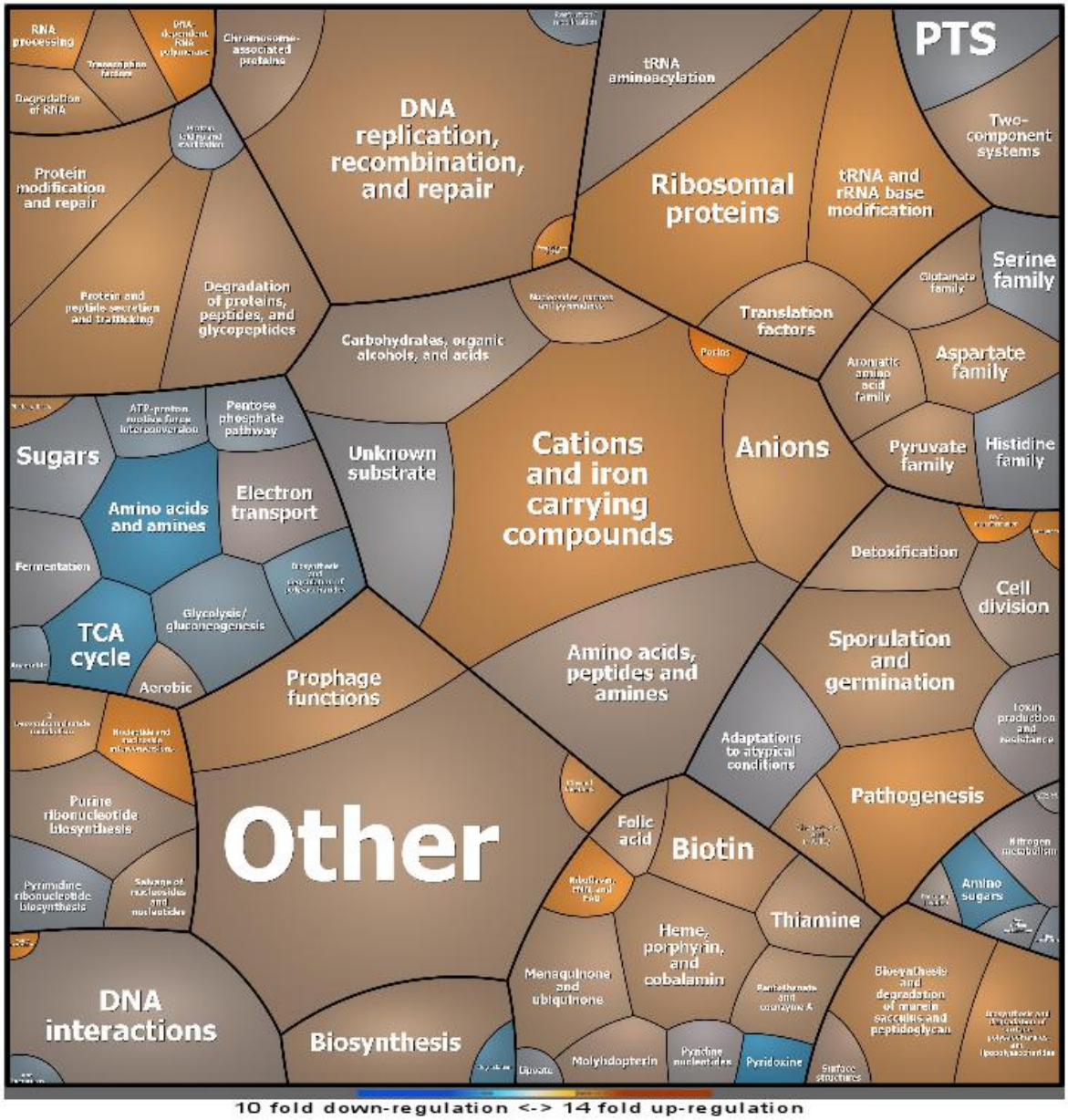
RNA processing
Degradation of RNA
Chromosome-associated proteins
DNA replication, recombination, and repair
tRNA aminoacylation
PTS
Two-component systems
Protein modification and repair
Ribosomal proteins
tRNA and rRNA base modification
Serine family
Protein and peptide secretion and trafficking
Degradation of proteins, peptides, and glycopeptides
Carbohydrates, organic alcohols, and acids
Translation factors
Glutamate family
Aspartate family
Aromatic amino acid family
Sugars
Pentose phosphate pathway
Unknown substrate
Cations and iron carrying compounds
Anions
Pyruvate family
Histidine family
Amino acids and amines
Electron transport
Detoxification
Fermentation
Cell division
TCA cycle
Glycolysis/ gluconeogenesis
Sporulation and germination
Amino acids, peptides and amines
Aerobic
Prophage functions
Adaptations to atypical conditions
Pathogenesis
Purine ribonucleotide biosynthesis
Other
Folic acid
Biotin
Amino sugars
Pyrimidine ribonucleotide biosynthesis
Thiamine
Heme, porphyrin, and cobalamin
Menaquinone and ubiquinone
DNA interactions
Biosynthesis
Molybdopterin
Pyridoxine
10 fold down-regulation <-> 14 fold up-regulation

Fig. 6

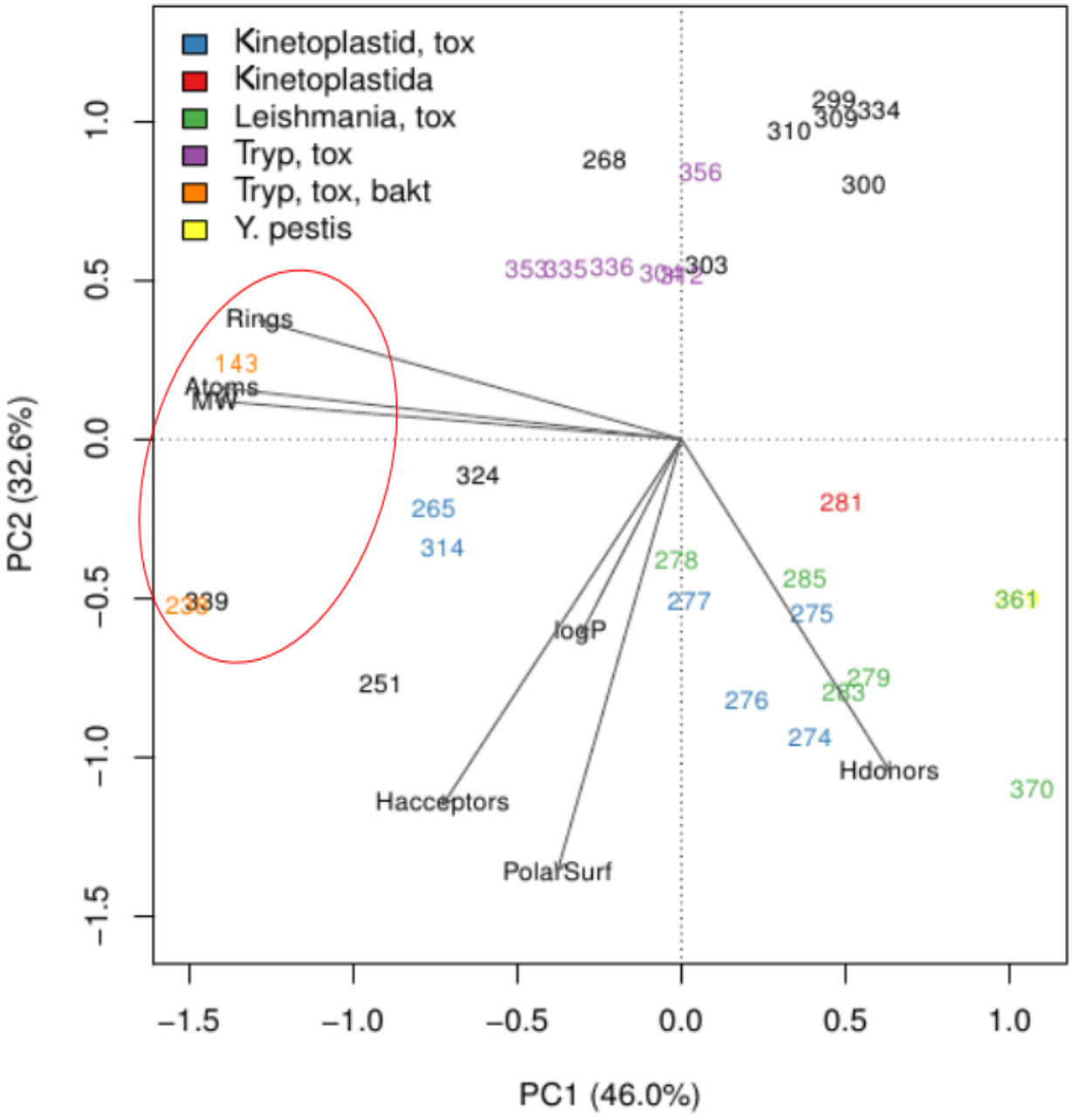
Kinetoplastid, tox
Kinetoplastida
Leishmania, tox
Tryp, tox
Tryp, tox, bakt
Y. pestis
PC2 (32.6%)
PC1 (46.0%)
1.0
0.5
0.0
−0.5
−1.0
−1.5
−1.5
−1.0
−0.5
0.0
0.5
1.0
Rings
143
Atoms
MW
339
251
324
265
314
268
356
303
299
334
309
310
300
281
278
285
277
275
361
279
276
274
Hdonors
370
logP
Hacceptors
PolarSurf

Fig. 7

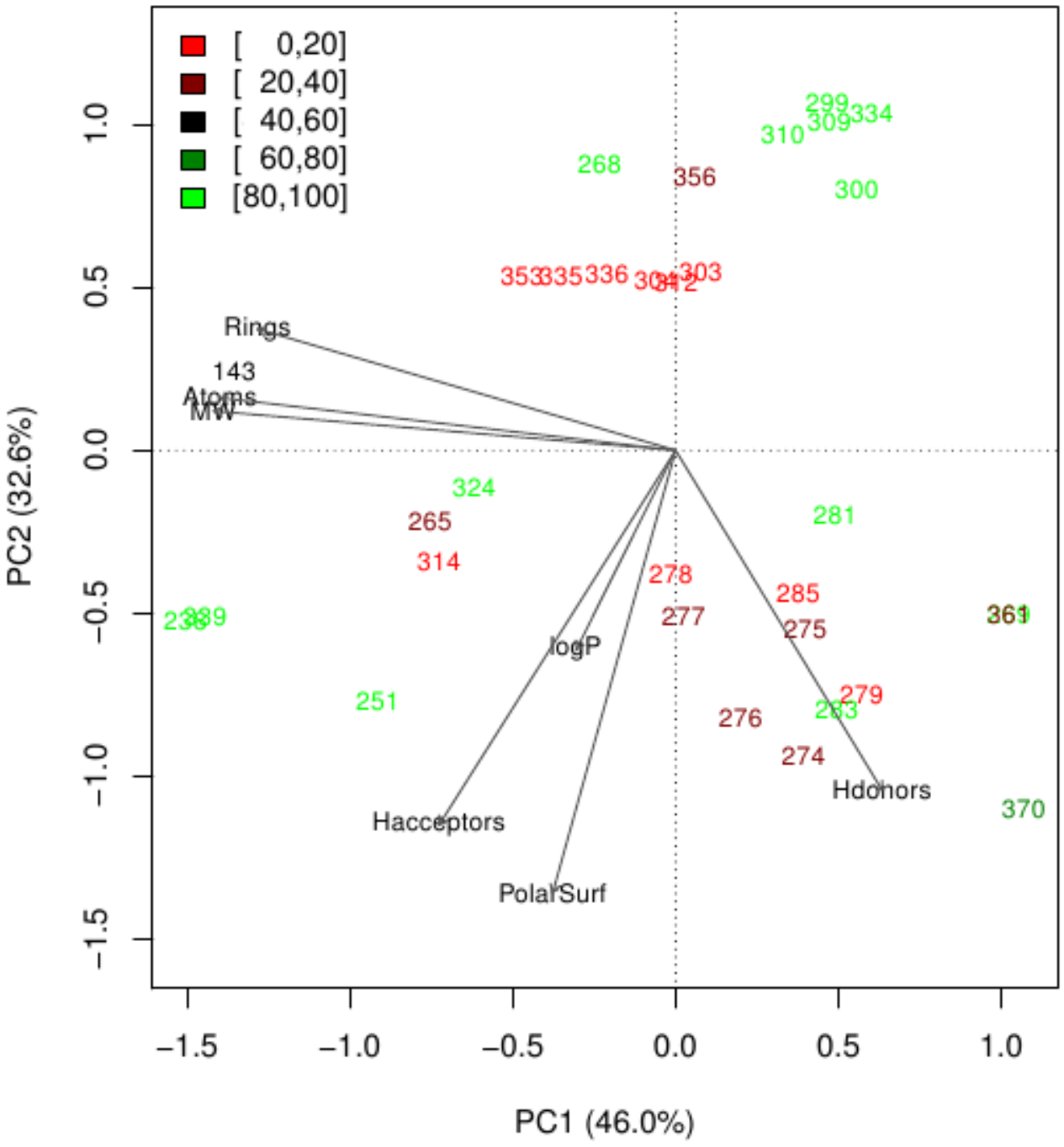
[0,20]
[20,40]
[40,60]
[60,80]
[80,100]
Rings
143
Atoms
MW
logP
Hacceptors
PolarSurf
Hdonors
PC1 (46.0%)
PC2 (32.6%)

Fig. 8

e-component

Click here to download e-component: IJMM_SUPPLEMENTARY_MATERIALSf.doc